Theoretical study of a novel intermediate temperature photovoltaic/thermal system equipped with heat pipe and evacuated tube

Xiao Ren[a], Gangqiang Dang[a], Liang Gong[a,*], Jing Li[b], Chuanyong Zhu[a], Xinyue Duan[a], Gang Pei[c,*]

[a] *College of New Energy, China University of Petroleum (East China), Qingdao, China*

[b] *Research Center for Sustainable Energy Technologies, Energy and Environment Institute, University of Hull, Hull, UK*

[c] *Department of Thermal Science and Energy Engineering, University of Science and Technology of China, Hefei, China*

[*]Corresponding author. E-mail address: lgong@upc.edu.cn; peigang@ustc.edu.cn

Abstract

Solar photovoltaic/thermal (PV/T) technology has enormous promise in the field of renewable cogeneration as a key technology to increase the utilization rate of solar energy. The structural restrictions of PV/T and the high power temperature coefficient of solar cells make PV/T mostly used in low-temperature situations. However, the combination of intermediate temperature PV/T and low-grade energy utilization devices can create a wider range of application values, including absorption refrigeration, seawater desalination, and the organic Rankine cycle. To increase the overall efficiency and thermal energy grade of the PV/T system, a novel heat pipe evacuated tube PV/T (HE-PV/T) system is proposed. The heat transfer is modeled using distributed parameters, and the thermoelectric performance and temperature uniformity are computed through numerical simulation. The impacts of different parameters on the thermodynamic performance of the HE-PV/T system are examined. Compared with traditional flat plate PV/T, the system's overall energy utilization efficiency and exergy efficiency have been significantly increased. When the inlet temperature is 80.0 °C, the overall energy and exergy efficiency of the HE-PV/T system can reach 33.55% and 7.92%, which is 29.66% and 21.97% higher than that of flat plate PV/T. Besides, the temperature distribution of the HE-PV/T is more uniform, which is beneficial for reducing thermal stress and mechanical damage. The property superiority and thermodynamic feasibility of the HE-PV/T system at medium temperature are demonstrated.

Keywords: Evacuated tube, Photovoltaic/thermal system, Distributed parameter model, Intermediate temperature, Temperature uniformity

Nomenclature

A	area, m^2
B	temperature coefficient, K^{-1}
c	specific heat capacity, J/(kg·K)
D	diameter of heat pipes， m
d	thickness, m
E	electrical gain, W
G	solar irradiance, W/m^2
h	heat transfer coefficient, W/(m^2·K)
L	length, m
M	mass, kg
m	mass flow rate, kg/s
Nu	Nusset number
Pr	Prandtl number
Q	heat gain, W
Re	Reynolds number
R	thermal resistance, m^2·K/W
T	temperature, K
V	volume, m^3

Greek letters

α	absorptivity
ε	emissivity
η	efficiency
ξ	covering factor
λ	thermal conduction, W/(m·K)
ρ	density, kg/m^3
σ	Stefan-Boltzmann constant, W/(m^2·K^4)
τ	transmittance

Subscripts

a	absorptivity
ad	adhesive layer
b	aluminum plate
c	cooling
cl	contact thermal resistance
cv	convective heat transfer
d	depth
e	evaporation
ele	electrical efficiency
eq	equivalent ambient
er	radiation heat transfer
exp	experiment
f	rib ridge width
g	glass tube
gd	Cross area of glass tube
i	inner diameter
in	water inlet
l	liquid
o	outside diameter
out	water outlet
p	heat pipe
part	part surface
PV	photovoltaic module
pvt	Photovoltaic/thermal
ref	standard test condition
sec	intersecting surface
sd	heat shield
sg	single
sim	simulation
sun	solar
TPT	Tedlar-Polyester-Tellar
t	tube
th	thermal
w	water
we	welding material
wk	wick
wt	cooling water volume

Abbreviations

HE-PV/T	heat pipe evacuated tube photovoltaic/thermal

1. Introduction

Improved solar energy system installation and higher solar utilization rates have long been the shared objectives of researchers in the sector of solar energy utilization[1]. Photovoltaic thermal (PV/T) technology is a combination of photovoltaic and thermal, where the collectors make photovoltaic cells cooled and capture the excess heat generated by the cells, so that the electricity and heat can be obtained at the same time[2,3]. At present, PV/T is mainly used in low-temperature areas with limited applications, such as air heating and domestic hot water. In contrast, the intermediate temperature PV/T system can combine with a wider range of uses[4], including combining absorption refrigeration[5,6], desalination[7,8], and organic Rankine cycle[9,10] power generation to realize the co-generation of cold-heat-power. The range of 75-90 °C is a common temperature of heat source for absorption chillers and organic Rankine cycle[11,12]. The combined way can not only meet the requirements of domestic heating, electricity, and cooling, but also highly enhance the comprehensive utilization rate of solar energy[13]. Especially in the western region of China, which has rich solar energy resources, it can not only provide residents with daily life energy, but also promote the development of carbon neutrality in China as a clean distributed energy output.

However, when the PV/T systems operate in medium and high temperatures, the solar cell type and system thermal stress are the important factors affecting the electrical performance and mechanical damage of the system, which mainly focus on the aspect of the battery power temperature coefficient and thermal expansion coefficient[14]. The crystalline silicon (c-Si) cells are the most used solar cells in low-temperature PV/T systems. But the high power temperature coefficient of roughly 0.4 to 0.6 %/°C is not conducive to medium temperature operation[15,16]. Particularly, there is a large difference in the thermal expansion coefficient between the c-Si cells and the aluminum plate (substrate), which can cause technical problems of structural deformation due to the large thermal stresses at fluctuating temperatures[17], and the system performance is affected[18]. Ulrich[17] used the finite element analysis to show The non-symmetrical structure of the complete photovoltaic module easily causes bending in the process of the thermal cycle. Fortunately, the amorphous silicon (a-Si) cells have been proven suitable for medium temperature operation, which performs low power temperature coefficient and long-term stability at medium temperature operation[19,20].

Moreover, the system structure is also a key factor in determining whether the medium temperature can be achieved. At present, the most common structure of PV/T system is the flat plate type, which performs a low thermal efficiency resulting in an operating temperature below 60.0 °C[21]. While the concentrating PV/T system can achieve medium temperature operation[22], it has the problems of complex structure and unstable operation, which require solar mirror field to cover a large area and is only suitable for large-scale sites[23,24]. The vacuum structure is a good choice to achieve medium temperature, which can effectively reduce convection and conduction heat loss. At present, the vacuum structure has been applied in the field of solar heat collection, such as evacuated flat plate collector and vacuum tube collector, and its medium temperature performance has been verified[25,26]. However, there are only a few studies on the evacuated PV/T system. A new vacuum flat plate PV/T with a vacuum layer atop the solar cells was conducted and compared to traditional PV/T, which shows higher thermal and electrical power additions[27], and by studying the effect of vacuum degree on the system performance, it is found that the higher the vacuum degree, the higher the thermal efficiency of the system, Xiao et al.[19] proposed an evacuated flat plate PV/T (FP-PV/T) system by using solar cells with positive power temperature coefficients, and the high-temperature performance of this system has been proved. In fact, the vacuum structure will produce a significant pressure difference on both sides of the glass cover, which will cause the glass cover to break. Besides, a significant tensile stress is present around the corner of the glass cover, which could lead to the glass cover breaking[28], which does not benefit the system's stability. To solve this problem, it is necessary to install the support pillars below the glass cover, but the support pillars will cast shadows on the solar cells, which will be detrimental to the electrical performance of the cells[29]. According to Wang's study[30], the frame shadow can result in a 39.3% reduction in photoelectric efficiency in the worst situation. Hence, to improve the effectiveness and stability of PV/T systems, it is necessary to reduce the shadow effect caused by the support structure and avoid large thermal stress.

In comparison, the vacuum tube structure requires less support structure and exhibits less thermal stress. Since the evacuated tube has a nearly streamlined surface, the pressure difference resistance generated between the circular tube surface and the atmosphere is small, so it does not need too much support structure to alleviate the pressure difference between the atmospheric environment and the internal vacuum. The characteristic of vacuum tube has been verified by Gao et al[31]. and the energy and exergy efficiency of solar collectors can also be enhanced in conditions of moderate temperature. Moreover, the axisymmetric structure of the circular tube makes the material distribution uniform, the stability in all directions is equal, the temperature distribution is uniform, and the thermal stress is small. A more uniform stress distribution is realized with the contribution of the tubular shape of the evacuated tube solar collector[32]. Tubular can therefore significantly reduce the system's thermal stress problem when applied to PV/T systems. At present, the vacuum tube PV/T system has not been actively promoted, despite the fact that the vacuum tube solar collector system has been used extensively in the field of medium temperature. The vacuum tube PV/T structure is a practical solution to increase system efficiency and reduce thermal stress, and the feasibility of the system has not been reported. Thus, it is necessary to elaborate on the system's thermodynamic issues to illustrate the reliability of the system.

To fill the research gap of the intermediate temperature PV/T system mentioned above, this paper proposes a new PV/T system structure, known as the heat pipe evacuated tube PV/T solar collector (HE-PV/T) using heat pipe, evacuated tube, and a-Si cells. However, the temperature stratification phenomenon at the junction of the battery and the heat-absorbing material is easily caused by the difference in thermal conductivity between both[33,34], resulting in the local temperature increase at the edge of the battery, thus affecting the cell’s power generation efficiency. In order to explore the temperature change during the working process of the two and investigate the heat transfer process of the HE-PV/T system, a relatively distributed parameter model with high precision is developed. The temperature distribution and uniformity of solar cells are revealed, and the system's energy quality is examined from the standpoint of exergy under various conditions. Finally, compared with traditional flat plate PV/T, the comprehensive energy efficiency and exergy efficiency of the novel HE-PV/T system are sharply enhanced, and the temperature distribution of cells is more uniform at medium temperature, which is a vital advantage to extend cells’ lifetime.

2. System description and working principle

Fig. 1 depicts the HE-PV/T structure and side view diagram, which comprises a heat exchanger, HE-PV/T, and supports. Glass tube, ethylene-vinyl acetate (EVA), a-Si solar cells, black Tedlar-polyester-tedlar (TPT), aluminum plate, heat pipe, and shield plate are the components of the HE-PV/T. The electrically insulating material black TPT can prevent cells from the shot circuit and enhance system absorptivity. A heat pipe is laser welded to the back of the aluminum plate, and its condenser section is inserted into a heat exchange. A vacuum environment is created inside the glass tube to reduce the heat convection and conduction on the solar cells' surface. As shown in Fig. 1 (b), The majority of solar radiation passing through the glass tube is absorbed by PV cells and black TPT; part of the radiation is converted into electricity and heat by the solar cells, while the rest is ultimately converted to heat energy by the black TPT. The heat is transferred from the cells layer to absorber plates by heat conduction and then transferred to the evaporator portion of the heat pipe, where it is absorbed by the cooling water through the pipes' condenser section and the heat exchanger.

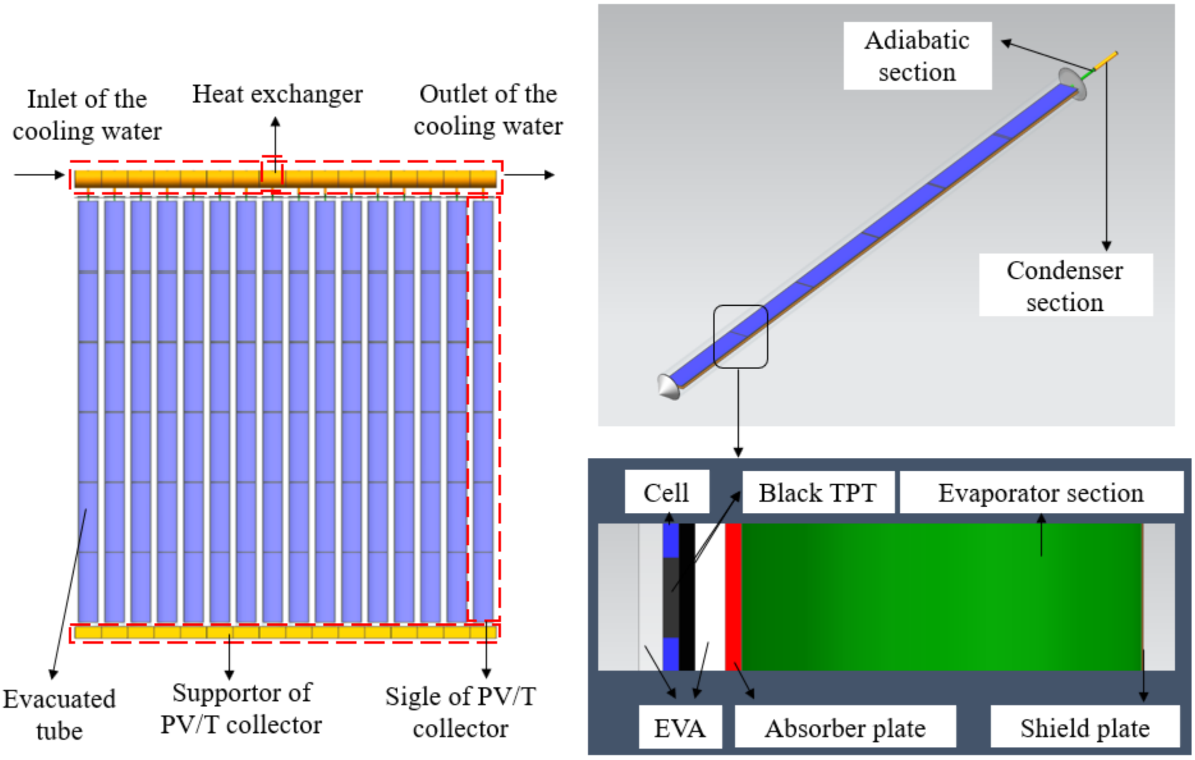

(a)

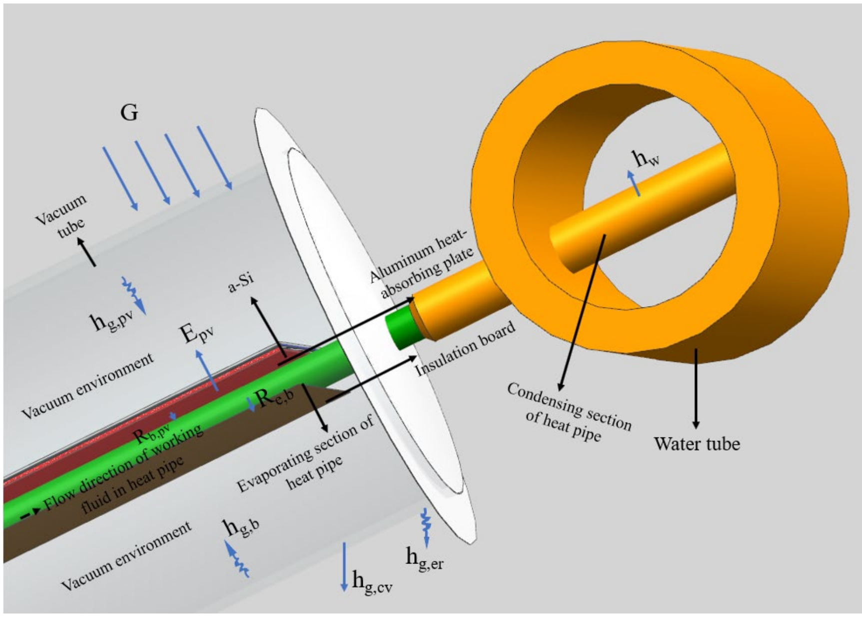

(b)

Fig. 1. (a) Structure diagram of the HE-PV/T collector; (b) heat transfer process of the HE-PV/T collector.

Glass tube, EVA, PV cell, black TPT, absorber plate, and shield plate have respective thicknesses of roughly 2.8 mm, 0.6 mm, 1.16 mm, 1.16 mm, 1 mm, and 0.8 mm. The HE-PV/T collector's structural dimensions are shown in Fig. 2. For the HE-PV/T collector, six a-Si cells with a size of 245 mm×88 mm are laminated on an absorber plate measuring 1960 mm×92 mm and built into a glass tube with the diameter and length of 102 mm and 2000 mm, where the cell's gap is 100 mm×92 mm. The length of the heat pipe's evaporator and condenser section is 1960 mm and 110 mm, respectively. And 16 vacuum tubes with identical configurations comprise the HE-PV/T collector. Its heat absorption area is 2.88 m^2 and it is placed at an angle of 30° to the ground.

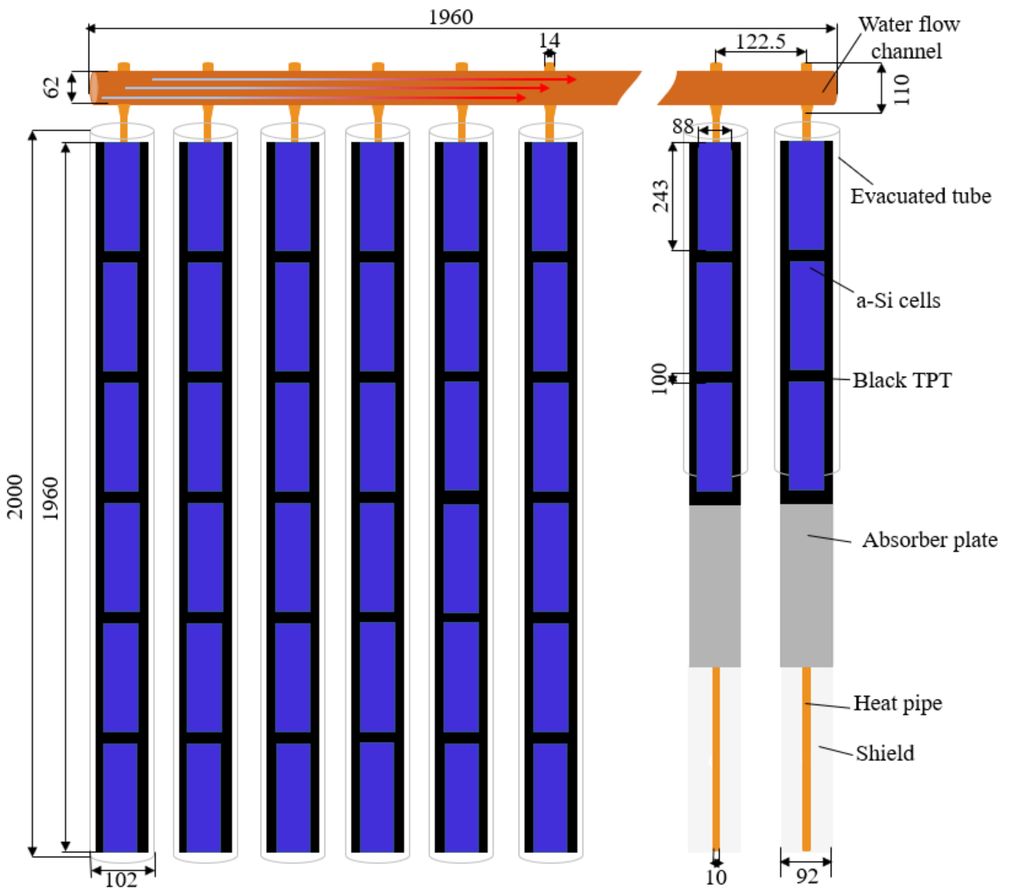

Fig. 2. Structural dimensions of the HE-PV/T.

It is noted that the HE-PV/T system's sealing of the vacuum tube has complex technical requirements, under long-term operation, it is simple to experience insufficient vacuum levels, which reduces system effectiveness. However, when there is a problem with a single tube, it will not affect the performance of the overall PV/T collector, which can reduce the difficulty and cost of maintenance. From a technical standpoint, the heat pipe type vacuum tube PV/T system has high feasibility and considerable cost, compared to the flat type vacuum PV/T system which needs a large area vacuum plate. The vacuum flat plate structure will produce a significant pressure difference on both sides of the glass cover, which will cause the glass cover to break. Thus, a large number of support columns are required, but it will produce shadows on the PV cells, which will be detrimental to the electrical performance of the cells. Fortunately, the vacuum tube structure presented in this paper requires less support structure. The performance of the novel HE-PV/T system in intermediate temperatures can be significantly improved.

3. Mathematic models

3.1 Mathematic models of the HE-PV/T system

This work develops a distributed parameter model to investigate the thermal and electrical performance of the novel HE-PV/T system. Compared with the lumped parameter model, a distributed parameter model can provide a better insight into the heat transfer and power conversion of the proposed system, especially the specifics of the temperature distribution of each component. The similar presumptions as the following.

(1) Thermal resistance is disregarded. Since the thickness of glass tubes, PV cells, absorber plates, and heat pipes are thin, the temperature of the exterior and inner walls are assumed to be identical.

(2) Glass tubes and heat pipes have a consistent temperature distribution in the radial direction.

(3) Sunlight enters the collector in the normal direction of the absorber plates.

(4) The absorber plates and glass tubes exhibit diffuse ash surface characteristics.

In order to demonstrate the temperature distribution of the module precisely, the parameter equations of PV cell and black TPT should be established one by one, where time and space are mutually independent variables. Similarly, the mathematical models of absorber plate welded with the heat pipe and without connection to the heat pipe are built respectively. Therefore, for the glass tube, PV cell, black TPT, absorber plate, heat pipe, and cooling water, the energy balance equations are expressed as:

$$\begin{aligned} V_{\mathrm{g}}\rho_{\mathrm{g}}c_{\mathrm{g}}\frac{\partial T_{\mathrm{g}}}{\partial t} &= \lambda_{\mathrm{g}}A_{\mathrm{gd}}\frac{\partial^2 T}{\partial x^2} + A_{\mathrm{g}}h_{\mathrm{g,cv}}(T_{\mathrm{a}} - T_{\mathrm{g}}) + h_{\mathrm{g,er}}(T_{\mathrm{eq}} - T_{\mathrm{g}}) + h_{\mathrm{g,pv}}(T_{\mathrm{pv}} - T_{\mathrm{g}}) \\ &+ h_{\mathrm{g,b}}(T_{\mathrm{b}} - T_{\mathrm{g}}) + GD_{\mathrm{g}}L_{\mathrm{g}}\alpha_{\mathrm{g}} \end{aligned} \quad (1)$$

$$\begin{aligned} V_{g}\rho_{g}c_{g}\frac{\partial T_{g}}{\partial t} &= \lambda_{g}A_{gd}\frac{\partial^2 T}{\partial x^2} + A_{g}h_{g,\mathrm{cv}}(T_{a} - T_{g}) + h_{g,er}(T_{eq} - T_{g}) + h_{g,TPT}(T_{TPT} - T_{g}) \\ &+ h_{g,\mathrm{b}}(T_{b} - T_{g}) + GD_{g}L_{g}\alpha_{g} \end{aligned} \quad (2)$$

$$\rho_{\mathrm{pv}}c_{\mathrm{pv}}d_{\mathrm{pv}}\frac{\partial T_{\mathrm{pv}}}{\partial t} = \lambda_{\mathrm{pv}}d_{\mathrm{pv}}\left(\frac{\partial^2 T_{\mathrm{pv}}}{\partial x^2} + \frac{\partial^2 T_{\mathrm{pv}}}{\partial y^2}\right) + h_{\mathrm{g,pv}}(T_{\mathrm{g}} - T_{\mathrm{pv}}) + \frac{T_{\mathrm{b}} - T_{\mathrm{pv}}}{R_{\mathrm{b,pv}}} + G(\tau\alpha)_{\mathrm{pv}} - E_{\mathrm{pv}} \quad (3)$$

$$\rho_{\mathrm{TPT}}c_{\mathrm{TPT}}d_{\mathrm{pv}}\frac{\partial T_{\mathrm{TPT}}}{\partial t} = \lambda_{\mathrm{TPT}}d_{\mathrm{pv}}\left(\frac{\partial^2 T_{\mathrm{TPT}}}{\partial x^2} + \frac{\partial^2 T_{\mathrm{TPT}}}{\partial y^2}\right) + h_{\mathrm{g,TPT}}(T_{\mathrm{g}} - T_{\mathrm{TPT}}) + \frac{T_{\mathrm{b}} - T_{\mathrm{TPT}}}{R_{\mathrm{b,TPT}}} + G(\tau\alpha)_{\mathrm{TPT}} \quad (4)$$

$$\rho_{\mathrm{b}}c_{\mathrm{b}}d_{\mathrm{b}}\frac{\partial T_{\mathrm{b}}}{\partial t} = \lambda_{\mathrm{b}}d_{\mathrm{b}}\left(\frac{\partial^2 T_{\mathrm{b}}}{\partial x^2} + \frac{\partial^2 T_{\mathrm{b}}}{\partial y^2}\right) + \frac{T_{\mathrm{pv}} - T_{\mathrm{b}}}{R_{\mathrm{b,pv}}} + \frac{T_{\mathrm{p,e}} - T_{\mathrm{b}}}{R_{\mathrm{e,b}}A_{\mathrm{b,sg}}} \quad (5)$$

$$\rho_{\mathrm{b}}c_{\mathrm{b}}d_{\mathrm{b}}\frac{\partial T_{\mathrm{b}}}{\partial t} = \lambda_{\mathrm{b}}d_{\mathrm{b}}\left(\frac{\partial^2 T_{\mathrm{b}}}{\partial x^2} + \frac{\partial^2 T_{\mathrm{b}}}{\partial y^2}\right) + \frac{T_{\mathrm{TPT}} - T_{\mathrm{b}}}{R_{\mathrm{b,TPT}}} + \frac{T_{\mathrm{p,e}} - T_{\mathrm{b}}}{R_{\mathrm{e,b}}A_{\mathrm{b,sg}}} \quad (6)$$

$$\rho_{\mathrm{b}}c_{\mathrm{b}}d_{\mathrm{b}}\frac{\partial T_{\mathrm{b}}}{\partial t} = \lambda_{\mathrm{b}}d_{\mathrm{b}}\left(\frac{\partial^2 T_{\mathrm{b}}}{\partial x^2} + \frac{\partial^2 T_{\mathrm{b}}}{\partial y^2}\right) + \frac{T_{\mathrm{pv}} - T_{\mathrm{b}}}{R_{\mathrm{b,pv}}} \quad (7)$$

$$\rho_{\mathrm{b}}c_{\mathrm{b}}d_{\mathrm{b}}\frac{\partial T_{\mathrm{b}}}{\partial t} = \lambda_{\mathrm{b}}d_{\mathrm{b}}\left(\frac{\partial^2 T_{\mathrm{b}}}{\partial x^2} + \frac{\partial^2 T_{\mathrm{b}}}{\partial y^2}\right) + \frac{T_{\mathrm{TPT}} - T_{\mathrm{b}}}{R_{\mathrm{b,TPT}}} \quad (8)$$

$$M_{\mathrm{p,e}}c_{\mathrm{p}}\frac{\partial T_{\mathrm{p,e}}}{\partial t} = (T_{\mathrm{p,c}} - T_{\mathrm{p,e}})/R_{\mathrm{e,c}} + (T_{\mathrm{b}} - T_{\mathrm{p,e}})/R_{\mathrm{e,b}} \quad (9)$$

$$M_{\mathrm{p,c}}c_{\mathrm{p}}\frac{\partial T_{\mathrm{p,c}}}{\partial t} = (T_{\mathrm{p,e}} - T_{\mathrm{p,c}})/R_{\mathrm{e,c}} + (T_{\mathrm{w}} - T_{\mathrm{p,c}})/R_{\mathrm{w,c}} \quad (10)$$

$$V_{\mathrm{wt}}\rho_{\mathrm{w}}c_{\mathrm{w}}\frac{\partial T_{\mathrm{w}}}{\partial t}=-m_{\mathrm{w}}c_{\mathrm{w}}\frac{\partial T_{\mathrm{w}}}{\partial x}+V_{\mathrm{wt}}\lambda_{\mathrm{w}}\frac{\partial^{2}T_{\mathrm{w}}}{\partial x^{2}}+(T_{\mathrm{a}}-T_{\mathrm{w}})/R_{\mathrm{w,a}}+(T_{\mathrm{p,c}}-T_{\mathrm{w}})/R_{\mathrm{w,c}} \tag{11}$$

where, the d, ρ, c, A, λ is the thickness (m), density (kg/m^3), specific heat capacity (J/kg·K), area (m^2), thermal conduction (W/m·K); h and R are the heat transfer coefficients (W/m^2·K) and thermal resistant (m^2·K/W); T is the temperature (K); t is the time (s); m is the mass flow rate (kg/s); M is the mass (kg); V is the Volume (m^3); G is the solar irradiance (W/m^2); ξ is the covering factor of the cells.

$h_{\mathrm{g,cv}}$ is the convective heat transfer coefficient between the glass tube and environments[35]; $h_{\mathrm{g,er}}$, $h_{\mathrm{g,pv}}$, $h_{\mathrm{g,TPT}}$ and $h_{\mathrm{g,b}}$ are the radiant heat transfer coefficient between the glass tube and sky, between the glass tube and PV cell, between the glass tube and black TPT, and between the glass tube and absorber plate[36], respectively; $h_{\mathrm{c,i}}$ is the condensing heat transfer coefficient between the medium and inner wall of the condenser, a calculation formula summarized by Husseina et al[37], and h_{w} is the heat transfer coefficient between cooling water and heat exchanger[38], expressed as:

$$h_{\mathrm{g,cv}}=Nu_{\mathrm{g,cv}}\frac{K_{\mathrm{g}}}{D_{\mathrm{g}}} \tag{12}$$

$$h_{\mathrm{g,er}}=\sigma(T_{\mathrm{eq}}^{2}+T_{\mathrm{g}}^{2})(T_{\mathrm{eq}}+T_{\mathrm{g}})/(\frac{1-\varepsilon_{\mathrm{g}}}{\varepsilon_{\mathrm{g}}A_{\mathrm{g}}}+\frac{1}{A_{\mathrm{g}}}) \tag{13}$$

$$h_{\mathrm{g,TPT}}=\sigma(T_{\mathrm{TPT}}^{2}+T_{\mathrm{g}}^{2})(T_{\mathrm{TPT}}+T_{\mathrm{g}})/(\frac{1-\varepsilon_{\mathrm{g}}}{0.5\varepsilon_{\mathrm{g}}A_{\mathrm{g}}}+\frac{1}{A_{\mathrm{TPT}}}+\frac{1-\varepsilon_{\mathrm{TPT}}}{\varepsilon_{\mathrm{TPT}}A_{\mathrm{TPT}}}) \tag{14}$$

$$h_{\mathrm{g,pv}}=\sigma(T_{\mathrm{pv}}^{2}+T_{\mathrm{g}}^{2})(T_{\mathrm{pv}}+T_{\mathrm{g}})/(\frac{1-\varepsilon_{\mathrm{g}}}{0.5\varepsilon_{\mathrm{g}}A_{\mathrm{g}}}+\frac{1}{A_{\mathrm{pv}}}+\frac{1-\varepsilon_{\mathrm{pv}}}{\varepsilon_{\mathrm{pv}}A_{\mathrm{pv}}}) \tag{15}$$

$$h_{\mathrm{g,b}}=\sigma(T_{\mathrm{g}}^{2}+T_{\mathrm{b}}^{2})(T_{\mathrm{g}}+T_{\mathrm{b}})/(\frac{1-\varepsilon_{\mathrm{g}}}{0.5\varepsilon_{\mathrm{g}}A_{\mathrm{g}}}+\frac{1}{A_{\mathrm{sd}}}+2\times\frac{1-\varepsilon_{\mathrm{sd}}}{\varepsilon_{\mathrm{sd}}A_{\mathrm{sd}}}+\frac{1}{A_{\mathrm{b}}}+\frac{1-\varepsilon_{\mathrm{b}}}{\varepsilon_{\mathrm{b}}A_{\mathrm{b}}}) \tag{16}$$

$$h_{\mathrm{c,i}}=[0.997-0.334(\cos\beta)^{0.108}][\frac{g\rho_{\mathrm{l}}^{2}k_{\mathrm{l}}^{3}h_{\mathrm{fg}}}{\mu_{\mathrm{l}}\Delta T_{\mathrm{cr}}L_{\mathrm{c}}}]^{0.25}[L_{\mathrm{c}}/D_{\mathrm{c,i}}]^{[0.254(\cos\beta)^{0.385}]} \tag{17}$$

$$h_{\mathrm{w}} = Nu_{w} \frac{k_{\mathrm{w}}}{D_{\mathrm{t}}} \tag{18}$$

$$Nu_{\mathrm{g,cv}} = 0.3 + \frac{0.62\,\mathrm{Re}^{1/2}\,\mathrm{Pr}^{1/3}}{[1+(0.4/\mathrm{Pr})^{2/3}]^{1/4}}[1+(\frac{\mathrm{Re}}{282000})^{5/8}]^{4/5} \tag{19}$$

$$Nu_{\mathrm{w}} = 0.3 + \frac{0.62\,\mathrm{Re}^{1/2}\,\mathrm{Pr}^{1/3}}{[1+(0.4/\mathrm{Pr})^{2/3}]^{1/4}}[1+(\frac{\mathrm{Re}}{282000})^{5/8}]^{4/5} \tag{20}$$

$$T_{\mathrm{eq}}^{4} = f_{\mathrm{sky}} \cdot T_{\mathrm{sky}}^{4} + f_{\mathrm{gr}} \cdot T_{\mathrm{gr}}^{4} + f_{\mathrm{gur}} \cdot T_{\mathrm{sur}}^{4} \tag{21}$$

$$T_{\mathrm{sky}} = 0.0552 \cdot T_{\mathrm{a}}^{1.5} \tag{22}$$

where β is the dip angle of the heat pipe, ρ_{l} is the density of saturated liquid in the heat pipe, h_{fg} is the latent heat of phase change of medium, μ_{l} is the dynamic viscosity of saturated liquid of medium, ΔT_{cr} is the temperature difference between medium and pipe wall. The qualitative temperature of the expression is decided by $(t_{\mathrm{w}}+t_{\infty})/2$, and is used for $RePr>0.2$. T_{sur}, T_{gr}, and T_{sky} represent the temperature of the surroundings, ground, and sky. f_{sur}, f_{gr}, and f_{sky} are their view factors[39], respectively.

$R_{\mathrm{b,pv}}$ and $R_{\mathrm{b,TPT}}$ are the thermal resistance between the PV cell and the absorber plate, and between the black TPT and the absorber plate; $R_{\mathrm{e,b}}$ and $A_{\mathrm{b,sg}}$ are the thermal resistance between the absorber plate and the evaporator section of the heat pipe, the superficial area of a control volume, expressed as:

$$R_{\mathrm{b,pv}} = d_{\mathrm{ad}} / \lambda_{\mathrm{ad}} \tag{23}$$

$$R_{\mathrm{b,TPT}} = d_{\mathrm{ad}} / \lambda_{\mathrm{ad}} \tag{24}$$

$$R_{\mathrm{e,b}} = d_{\mathrm{we}} / (\lambda_{\mathrm{we}} A_{\mathrm{we}}) \tag{25}$$

$$A_{\mathrm{b,sg}} = dx \times L_{\mathrm{b}} \tag{26}$$

About the calculation of the heat pipe, the energy from the evaporator section into the condenser section is calculated using the total thermal resistance $R_{e,c}$. Reference[40] confirmed that the pressure drop of the vapor along the axial direction is very small and that the temperature of the working fluid is considered to be a constant number along the axial direction when the vapor space operates at a constant saturation pressure. The $R_{e,c}$ can be thought of as consisting of four basic parts: $R_{e,p}$ is the conductive heat resistance of the evaporator radial direction; $R_{e,i}$ is the equivalent heat resistance caused by the capillary core of the heat pipe evaporator; $R_{c,i}$ is the condensation resistance in the condenser section of the heat pipe, and $R_{c,p}$ is the conductive resistance of the condenser radial direction. And $R_{w,c}$ is the total thermal resistance between cooling water and the condensing wall of the heat pipe. As for the heat pipe's evaporator section, Fig. 3 demonstrates the inner structure of and a groove is used to accommodate the wick, λ_{wick} is the heat pipe wick's equivalent thermal conductivity[41]. The total resistance of the heat pipe is calculated by:

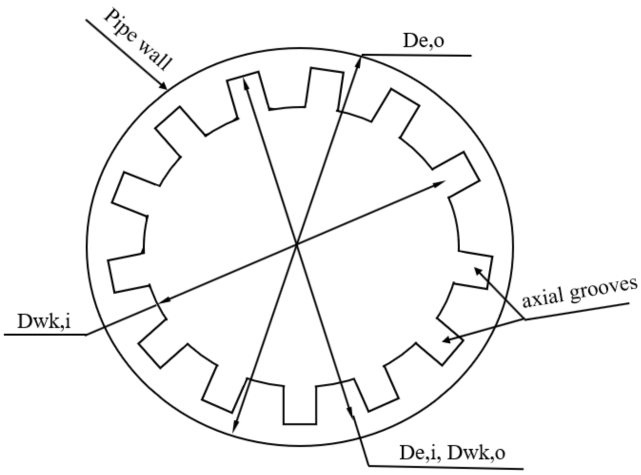

Fig. 3. Inner structure of the evaporator section.

$$R_{e,c} = R_{e,p} + R_{e,i} + R_{c,i} + R_{c,p} \tag{27}$$

$$R_{e,p} = \frac{\ln(D_{e,o} / D_{e,i})}{2\pi L_e \lambda_p} \tag{28}$$

$$R_{e,i} = \frac{\ln(D_{wk,o} / D_{wk,i})}{2\pi L_e \lambda_{wick}} \tag{29}$$

$$R_{c,i} = \frac{1}{\pi D_{c,i} L_c h_{c,i}} \tag{30}$$

$$R_{c,p} = \frac{\ln(D_{c,o} / D_{c,i})}{2\pi L_c k_p} \tag{31}$$

$$R_{w,c} = R_{cl} + \frac{1}{A_w h_w} \tag{32}$$

$$\lambda_{wick} = \frac{(w_f \lambda_l \lambda_{wk}) + w\lambda_l (0.185 w_f \lambda_{wk} + \lambda_l w_d)}{(w + w_f)(0.185 w_f \lambda_{wk} + \lambda_l w_d)} \tag{33}$$

where, R_{cl} is the contact thermal resistance between the heat exchanger and condensing wall of the heat pipe, A_w is the equivalent heat transfer area between cooling water and heat exchanger, λ_l and λ_{wk} are the conductive heat coefficient of liquid medium and material about wick. w_f is the width of the rib ridge of the channel, w and w_d are the width of the channel and the depth of the channel.

The $(\tau\alpha)_{pv}$ and $(\tau\alpha)_{TPT}$ are the effective absorptance efficiency of the PV cell, and the black TPT[36], E_{pv} is the electrical energy of the PV cell, expressed as:

$$(\tau\alpha)_{pv} = \tau_g \tau_{ad} \alpha_{pv} \tag{34}$$

$$(\tau\alpha)_{TPT} = \tau_g \tau_{ad} \alpha_{TPT} \tag{35}$$

$$E_{pv} = G\tau_g \tau_{ad} \eta_{ref} [1 - B(T_{pv} - T_{ref})] \tag{36}$$

where η_{ref} is the photovoltaic efficiency of the PV cell at standard test temperature T_{ref}=298.15 K, B is the power temperature coefficient of a-Si[42], 0.002 K^{-1}.

3.2 Performance evaluation

The thermal efficiency, electrical efficiency, and comprehensive energy efficiency[43] of the HE-

PV/T system can be defined as:

$$\eta_{\mathrm{th}} = \frac{Q_{\mathrm{w}}}{GA_{\mathrm{b}}} = \frac{c_{\mathrm{w}} m_{\mathrm{w}} (T_{\mathrm{out}} - T_{\mathrm{in}})}{GA_{\mathrm{b}}} \tag{37}$$

$$\eta_{\mathrm{pv}} = \frac{E_{\mathrm{pv}}}{GA_{\mathrm{pv}}} \tag{38}$$

$$\eta_{\mathrm{pvt}} = \eta_{\mathrm{th}} + \xi \frac{\eta_{\mathrm{pv}}}{\eta_{\mathrm{power}}} \tag{39}$$

where Q_{w} is the quantity of heat obtained by cooling water, m_{w} is the mass flowing rate of which, T_{in} and T_{out} are the inlet and outlet temperatures of the system, η_{power} is the electrical efficiency of the traditional thermal power plants, about 38%.

The second law of thermodynamics may assess the quality of energy flux, and exergy assesses the most productive amount of effort that can be done to bring the system and environment into total equilibrium, therefore, which can forecast how much work can be done in a system. Thermal exergy depends on the temperature and how much heat is generated, while electrical energy is pure exergy only depends on the size of electricity, which can be expressed as[44]:

$$Ex_{\mathrm{th}} = Q_{\mathrm{w}} (1 - \frac{T_{\mathrm{a}}}{T_{\mathrm{m}}}) \tag{40}$$

$$Ex_{\mathrm{pv}} = E_{\mathrm{pv}} \tag{41}$$

$$\eta_{\mathrm{ex,th}} = \frac{\sum Ex_{\mathrm{th}}}{\sum Ex_{\mathrm{G}} A_{\mathrm{b}}} \tag{42}$$

$$\eta_{\mathrm{ex,pv}} = \frac{\sum Ex_{\mathrm{pv}}}{\sum Ex_{\mathrm{G}} A_{\mathrm{pv}}} \tag{43}$$

$$\eta_{\mathrm{ex,pvt}} = \eta_{\mathrm{ex,th}} + \xi \eta_{\mathrm{ex,pv}} \tag{44}$$

Exergy of solar radiation incidents on PV/T collector per square meter and T_{m} (the log mean thermodynamic temperature difference between the inlet and outlet of cooling water.) can be expressed as:

$$Ex_{\mathrm{G}} = G(1 - \frac{T_{\mathrm{a}}}{T_{\mathrm{sun}}}) \quad (45)$$

$$T_{\mathrm{m}} = \frac{T_{\mathrm{out}} - T_{\mathrm{in}}}{\ln(T_{\mathrm{out}} / T_{\mathrm{in}})} \quad (46)$$

where T_{sun}=5760 K is the sun's surface temperature.

To evaluate the degree of agreement between the simulation and the experiment, the relative error[45] (RE) is calculated by:

$$RE = \frac{X_{\mathrm{exp}} - X_{\mathrm{sim}}}{X_{\mathrm{exp}}} \times 100\% \quad (47)$$

where the X_{exp} *and* X_{sim} *are the values of the experiment and simulation, respectively.*

3.3 Discretization of equations and numerical simulation

Fig. 4 depicts the grid division of the HE-PV/T system, and the axial direction of the heat pipe is the X-axis, while the direction of the cooling water is the Y-axis. Along the axis of each heat pipe, the temperature of the solar cells and aluminum plate is distributed symmetrically. The discrete nodes of the evaporation portion of the heat pipe and the vacuum tube are separated into i×j =47×1, and the discrete nodes of the PV module and the aluminum plate are divided into i×j =47×23, i×j =16×1 nodes are established for the grid discretization for the heat exchanger. Fig. 4 illustrates the outcome's type of the thermodynamic behavior of the two-dimensional region in the dotted box to represent its temperature distribution in the comprehensible contour plot format.

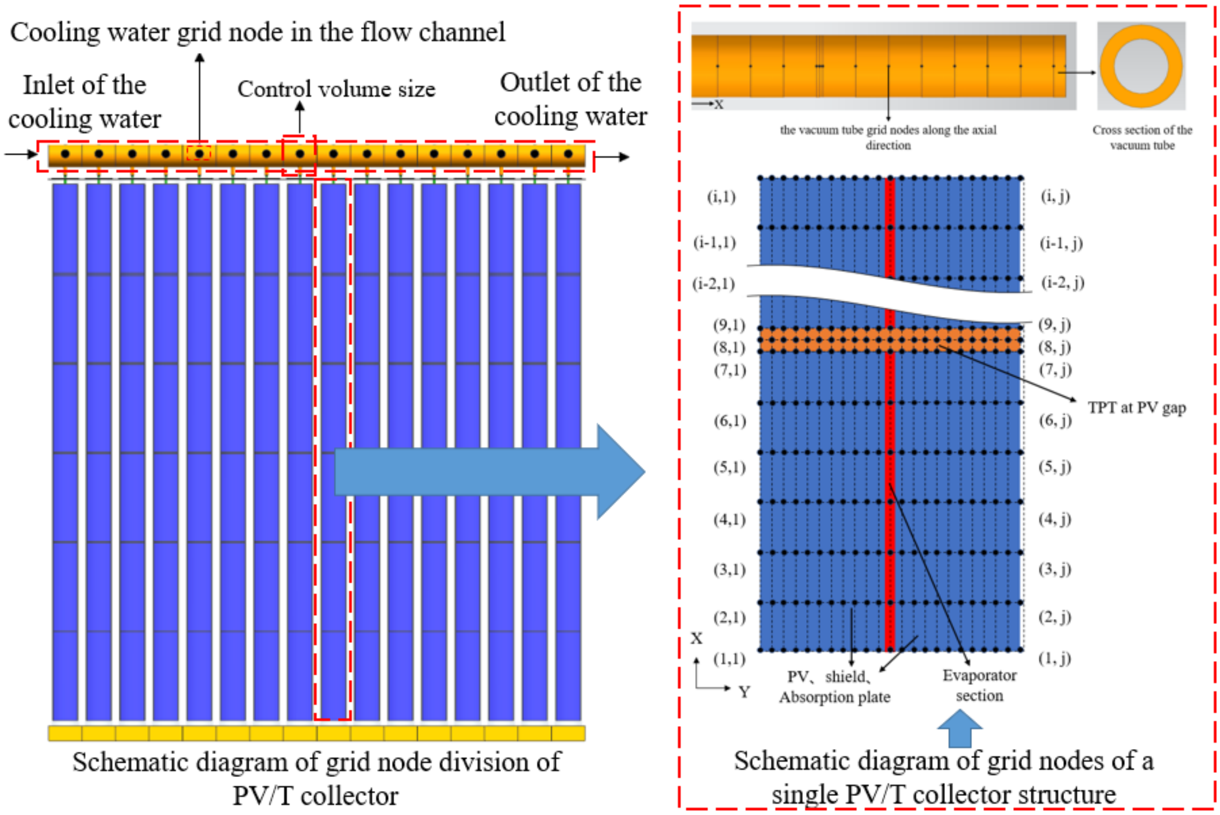

Fig. 4. The grid division of the HE-PV/T system.

All of the energy balance equations in this study are solved using discrete techniques. The second-order central difference approach is used to solve the energy balance equations of the vacuum tube, a-Si cell, aluminum plate, and the heat pipe's evaporation portion. First-order upwind discretization is employed for the water in the heat exchanger because it takes into consideration the effect of the incoming flow direction of the cooling water temperature in the flow channel. The mathematical discrete equations are solved by MATLAB programming, and the system settings are then optimized by analyzing the numerical results. The procedure for numerical simulation in this paper is shown in Fig. 5. It is necessary to enter the geographic location, meteorological factors, and inlet temperature in advance to solve the system's mathematical equation. Hefei is used as an example site for the simulation, and the time step is set to 2s. When the relative error of the calculation results between two times nodes is less than 10^{-5}, the system reaches a stable state, and the computation is finished.

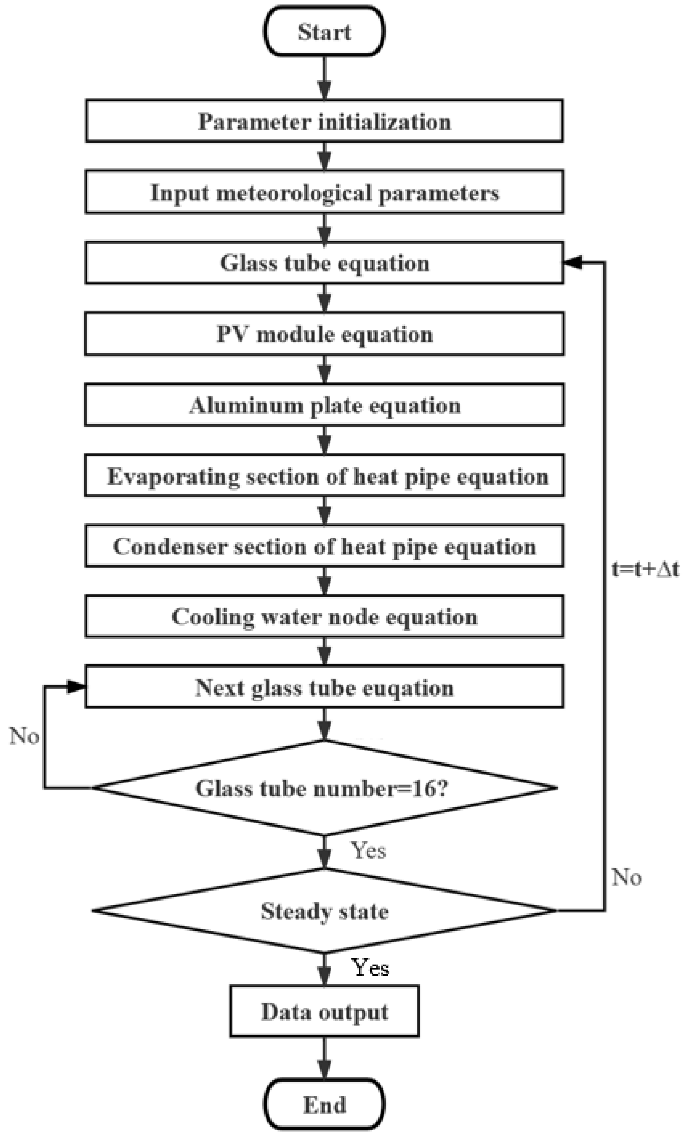

Fig. 5. Flow chart of the numerical simulation process.

3.4 Model validation

Since the system is a novel structure, there is no experimental data for model verification. In this section, the thermal model is validated with a heat pipe evacuated tube photothermal (PT) collection system[46], and the specific model construction is shown in Fig. 6. In order to confirm the accuracy of the calculation approach, the experimental data of the PT collector are compared with the numerical simulation findings in this work. The experimental site of the collector is determined to be in Hefei, China, at 31.9 °N and 117.3 °E, with a collector inclination angle of 30 °, cooling water flow of 0.035 kg/s, ambient temperature of 6.0 °C, and solar irradiation of 820 W/m^2 as the experimental parameters in the study. When the temperature is less than 250.0 °C, the heat absorber plate has an absorptivity and an emissivity of 0.95 and 0.1, respectively. Additionally, the discrete equation of the established fully hidden scheme is solved using point iteration to produce the five-diagonal matrix.

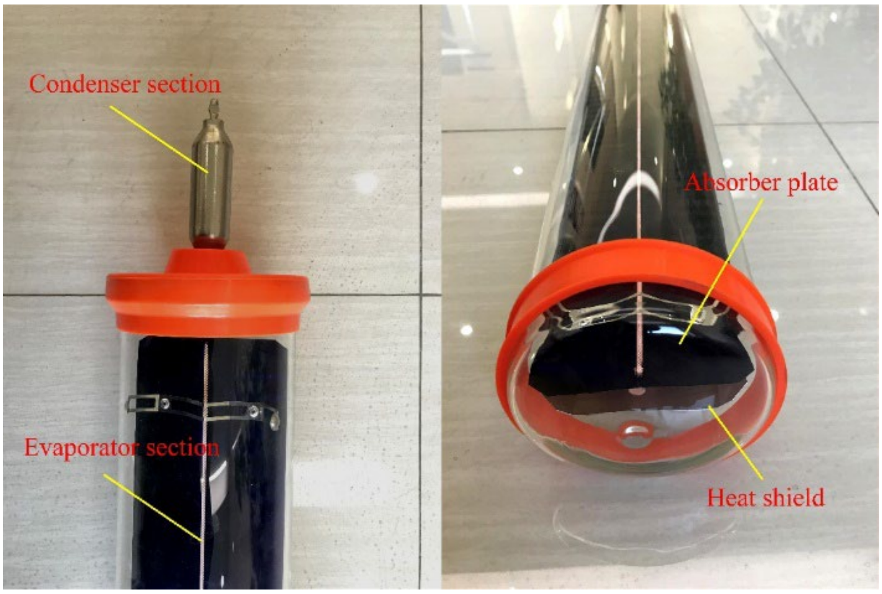

Fig. 6. Photograph of PT collector.

3.4.1 Grid independence test

To verify that the grid is independent of the numerical results, fixing the structural characteristics of the system, Fig. 7 (a) illustrates how the number of grids affects the system's thermal efficiency when the ambient wind speed is 2.5 m/s. The thermal efficiency drops from 80.85% to 77.46% when the number of grids is increased from 1936 to 26128, especially once the number of grids reaches 11408, the thermal efficiency is 77.46%, and the change of thermal efficiency is quite small. However, as the number of grids increases, calculation time will increase significantly. With regard to the accuracy and speed of the calculation, 11408 grids are selected for this calculation.

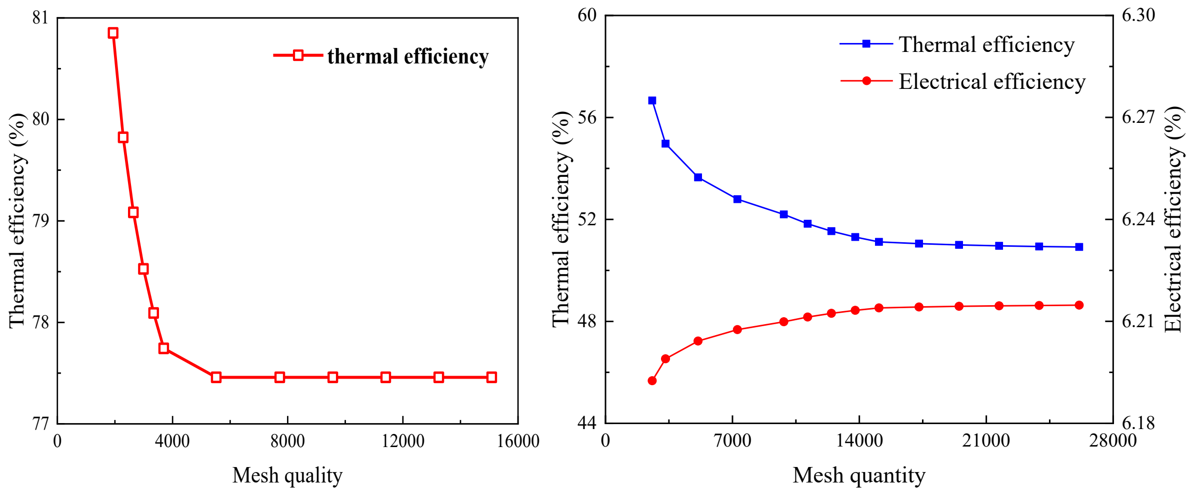

(a) (b)

Fig. 7. Grid independence test (a) PT system; (b) HE-PV/T system.

3.4.2 Simulation verification

The entrance temperature of the collector is raised from 18.8 °C to 147.6 °C when keeping all other parameters constant. To guarantee the applicability of the experimental findings, simulations, and experiments were performed four times at each inlet temperature. Figs. 8-10 display the temperature difference between the system's input and output, the heat gain, and the thermal efficiency of the PT system.

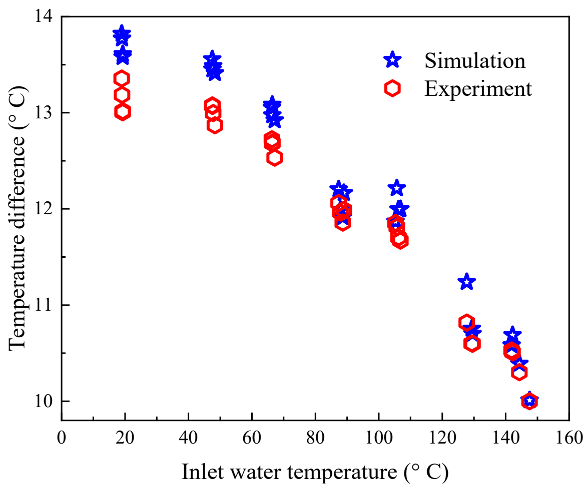

Fig. 8. Temperature difference between the inlet and outlet water temperature.

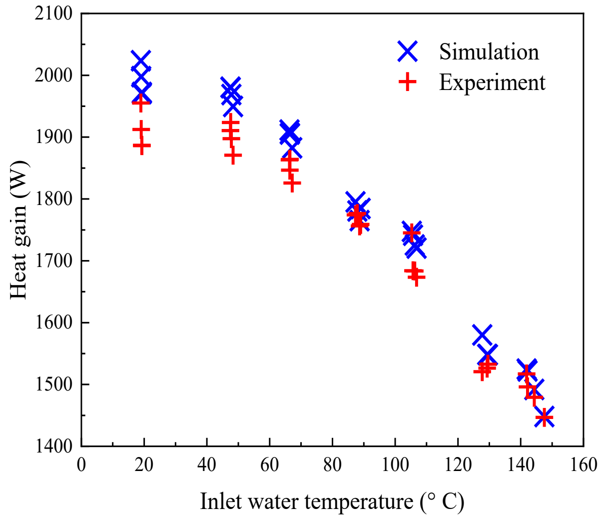

Fig. 9. Heat gain of the PT system.

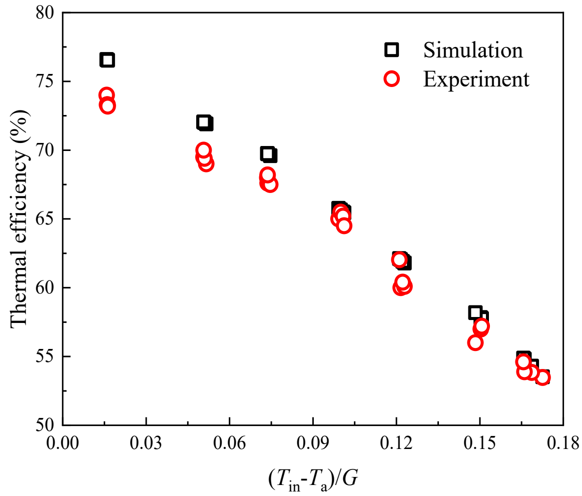

Fig. 10. Thermal efficiency of the PT system.

The temperature of the absorbing plate rises as the inlet water temperature rises. The heat transfer through the heat pipe will gradually decrease as the temperature of the absorbing plate rises under the same solar irradiance, in order to maintain the temperature stability of the absorbing plate. Figs. 8 and 9 show a downward trend in the temperature difference between the system's inlet and outlet and the heat gain, and Fig. 10 displays that the standardized temperature at the system's entrance rises from 0.016 to 0.173, the thermal efficiency falls from 74.00% to 53.47% in the experimental data, and from 76.58% to 53.52% in the simulated data. The maximum relative error of the two is 4.35% when the standardized inlet temperature is 0.016, and the error of the two also shows a downward trend with an increase in standardized inlet temperature. The simulation results are verified within the allowable error range, indicating that this calculation method can be used in both medium and low-temperature ranges. Thus, this method is used in this paper to resolve the energy balance equations.

4. Results and discussion

As a brand-new intermediate temperature PV/T system, HE-PV/T's working performance, energy flow process, temperature uniformity of the battery layer, and the impact of various working parameters on thermal efficiency, electrical efficiency, and exergy efficiency are still unknown. The high-precision mathematical model of the newly developed HE-PV/T system has been verified and has a high accuracy. In order to find out the medium temperature performance of the HE-PV/T system under typical daily conditions and its variation rule with different parameters, in the following section, numerical simulation will be done and the calculated results will be compared with FP-PV/T system. By changing the parameters such as ambient temperature, solar irradiance, inlet temperature, mass flow rate, and PV coverage rate, the changing law of system performance is demonstrated.

4.1 Performance evaluation of the HE-PVT system

To obtain the overall performance of the HE-PV/T system in operation, the thermal and electrical performance of the system under different inlet temperatures are simulated based on typical meteorological parameters. As shown in Fig. 11, the solar irradiation first increases and then decreases, reaching a maximum value at noon with a value of 1011W/m^2. The daily total solar irradiation is 47.7 MJ/m^2. The ambient temperature varies from 20.3 °C to 28.4 °C and the average ambient temperature is about 25.7 °C.

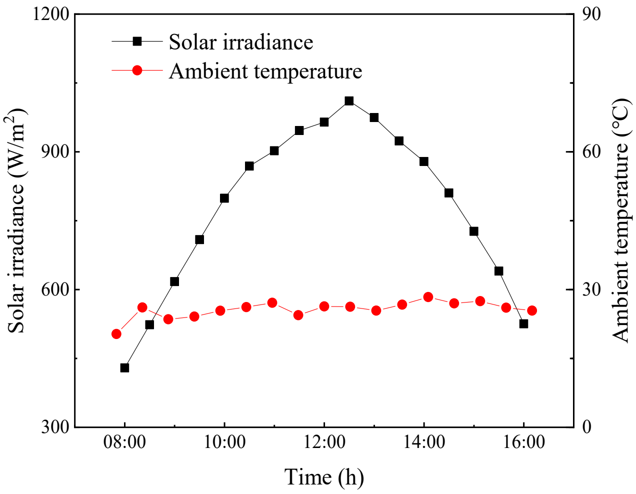

Fig. 11. Solar irradiance and ambient temperature change.

Full-day simulation results of the HE-PV/T system at the inlet water temperature of 60 °C, 70 °C, and 80 °C are presented in this section. As shown in Fig. 12, the temperature difference between the inlet and outlet of the system is consistent with the variation trend of solar irradiation. The higher the inlet temperature, the greater the heat loss between the collector and the environment, resulting in a lower temperature difference between the inlet and outlet. When the inlet water temperature is 60 °C, 70 °C, and 80 °C, the maximum temperature differences between the inlet and outlet are 7.4 °C, 6.3 °C, and 5.3 °C, respectively. Fig. 13 presents the simulation results of the thermal and electrical efficiency of the HE-PV/T system. The variation of the thermal efficiency is identical with the solar irradiation, and the thermal efficiency is highest at noon. However, due to the negative power temperature coefficient of the solar cell, the electrical performance decreases slightly at noon. With the increasing inlet water temperature, the thermal efficiency and electrical efficiency decrease, but even if the inlet water temperature is 80 °C, the thermal efficiency and electrical efficiency can still reach 32.02% and 5.49%. The comprehensive energy and exergy performance of the HE-PV/T system is shown in Fig.

14. When the inlet water temperature is 60 °C, 70 °C, and 80 °C, the maximum comprehensive energy efficiency of the HE-PV/T system reaches 55.20%, 48.68%, and 41.96%. The energy efficiency decreases with increasing inlet temperature, which is different from the trend of exergy efficiency. Among them, the exergy efficiency of the system at an inlet temperature of 70 °C is the highest with a value of 9.66%. This is because less heat is obtained when the inlet temperature rises, resulting in a decrease in the thermal efficiency of the system, on the contrary, the energy quality of the system can be enhanced as the operating temperature increases. This opposite effect on thermal exergy efficiency is more significant under the conditions of high solar irradiation and low ambient temperature, but the electrical exergy efficiency is declining slowly, as shown in Fig. 15.

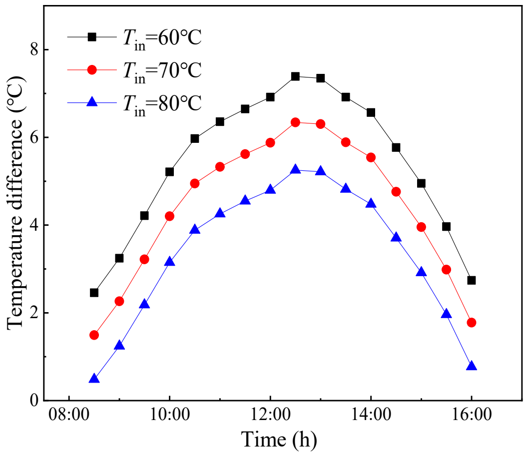

Fig. 12. Temperature difference between the inlet and outlet water temperature of the HE-PV/T system.

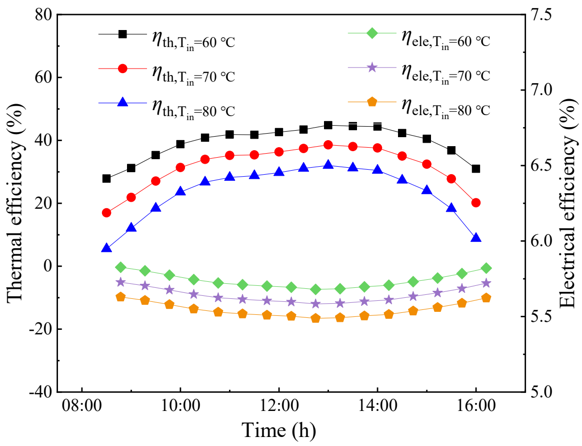

Fig. 13. Thermal and electrical efficiency of the HE-PV/T system.

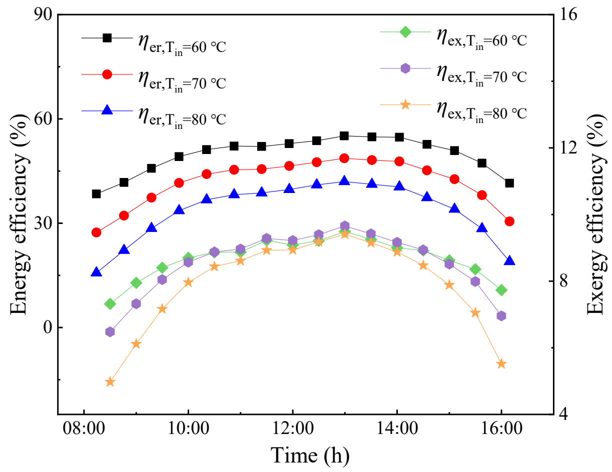

Fig. 14. Overall energy and exergy efficiency of the HE-PV/T system.

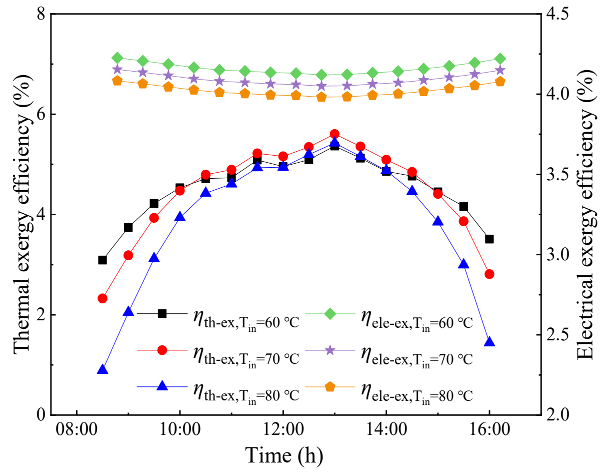

Fig. 15. Thermal and electrical exergy efficiency of the HE-PV/T system.

The temperature uniformity of the solar cell and absorber plate in a PV/T system has a significant impact on system performance. A drop in temperature can significantly reduce the likelihood of fracture brought on by mechanical stress loss[31]. As shown in Fig. 16, the temperature distributions of the PV module and the absorber plate at the solar irradiation of 600 W/m^2, the inlet temperature of 60.0 °C, the ambient temperature of 25.0 °C, and the ambient wind speed of 2 m/s are presented. Numbers 1 and 16 represent the first collector tube at the inlet of the collector and the last collector tube at the outlet. The average temperatures of the numbers 1 and 16 PV modules are 65.4 °C and 67.3 °C, and the value of the numbers 1 and 16 absorber plates are 64.9 °C and 66.9 °C, respectively. The maximum temperature difference of the cell is 0.6 °C varied from 64.5 °C to 65.1 °C. Compared with the FP-PV/T collector, the HE-PV/T system performs a more uniform temperature distribution. The uniform temperature distribution of the absorber plate will reduce the occurrence of solar cells falling off due to thermal stress loss, the security of the system has been greatly enhanced, and greatly extend the battery life.

Moreover, Fig. 17 presents the energy flow of the HE-PV/T system to visually convey the conversion process of solar radiation energy into usable energy and dissipation loss in the PV/T system. The system gets 1919.23 W of solar radiation energy, generates 69.43 W of electricity and 578.80 W of heat, and realizes the conversation of 33.78% of solar radiation into useful energy when the ambient temperature, inlet temperature, solar irradiance, and mass flow rate are 25.0 °C, 60.0 °C, 600 W/m^2, and 0.044 kg/s. In the process of energy flow, the total optical loss and the total radiation loss are 317.63 W and 768.98 W, occupying 16.55% and 40.06% of received solar energy, respectively.

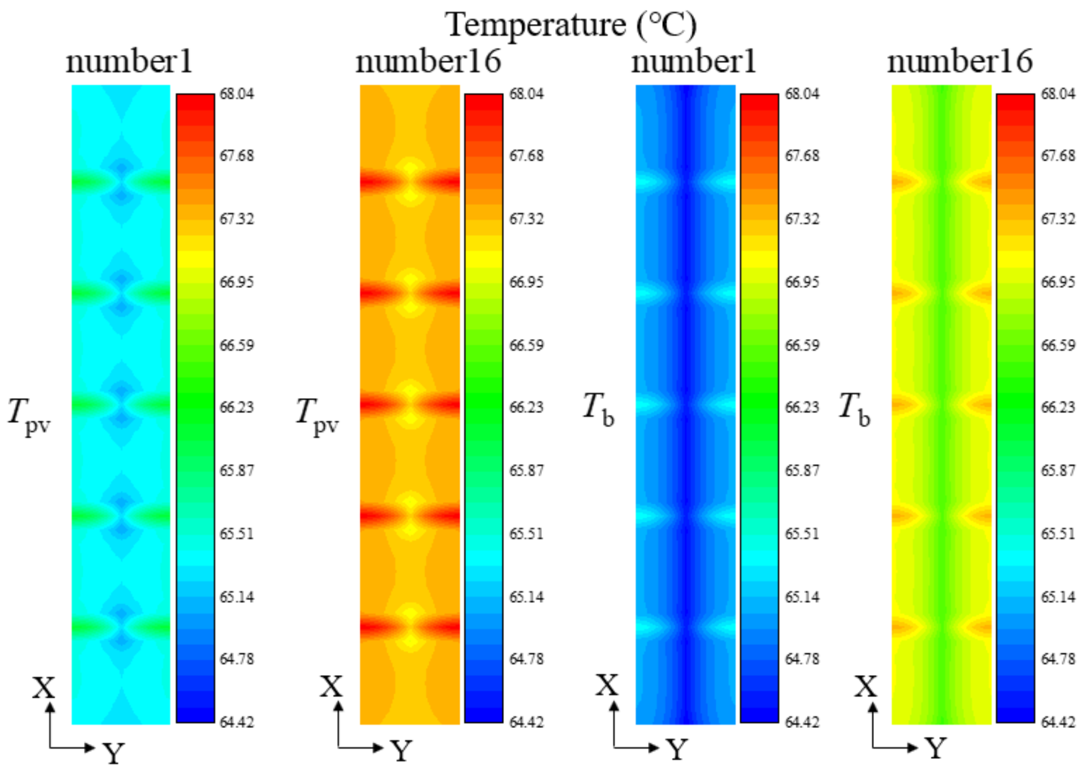

Fig. 16. Temperature distributions of the PV module and the absorber plate.

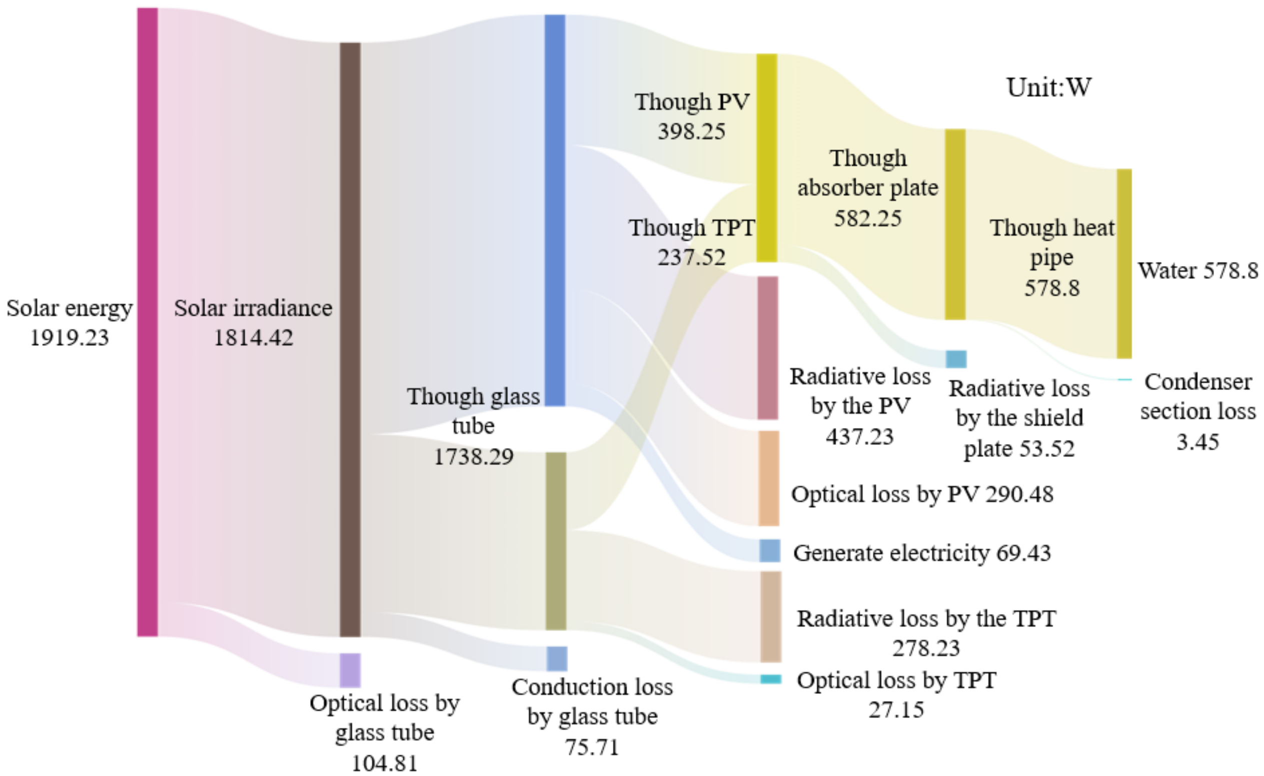

Fig. 17. The energy flow chart of the HE-PV/T system.

To evaluate the system performance at medium operating temperature, the full-day thermal and electrical performance of the HE-PV/T system compared with the FP-PV/T system is presented in Table 1. The parameters include thermal efficiency, electrical efficiency, energy efficiency, and exergy efficiency. When the inlet temperature is 80.0 °C, the overall energy and exergy efficiency of the HE-PV/T system can reach 33.55%, 7.92%, while the values of the FP-PV/T system are only 23.60%, 6.18%. The results show that the energy utilization rate and grade of the system have been greatly improved.

The annual electricity and heat of the system is an important index to evaluate the feasibility of the system, which can not only comprehensively reflect the system performance, but also evaluate the system design scheme in combination with economic and technical indicators. To obtain the annual profits of the system, this paper takes Hefei as a reference location and obtains its annual meteorological parameters from EnergyPlus software, as shown in Fig 18. After calculation, the monthly power generation and heat production of the HE-PV/T system can be obtained. As shown in Fig 19, the power generation and heat production in October are the highest (52.63 MJ and 179.4 MJ, respectively); the lowest (6.36 MJ and 15.82 MJ, respectively) in January; the annual power and heat production of the system are 387.557 MJ and 1234.332 MJ (107.65 kWh and 342.86 kWh), respectively; it can be seen that the system has the highest income during operation from April to November.

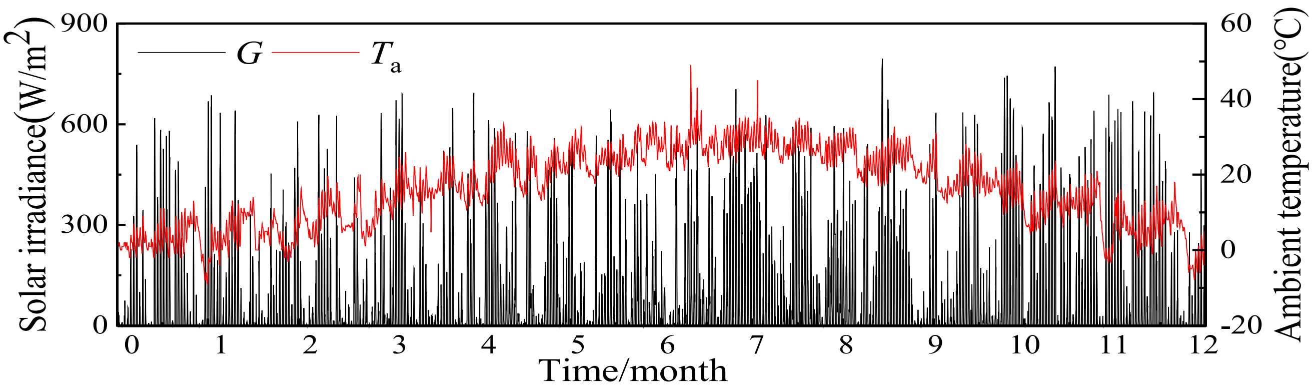

Fig. 18. Annual meteorological parameters of Hefei.

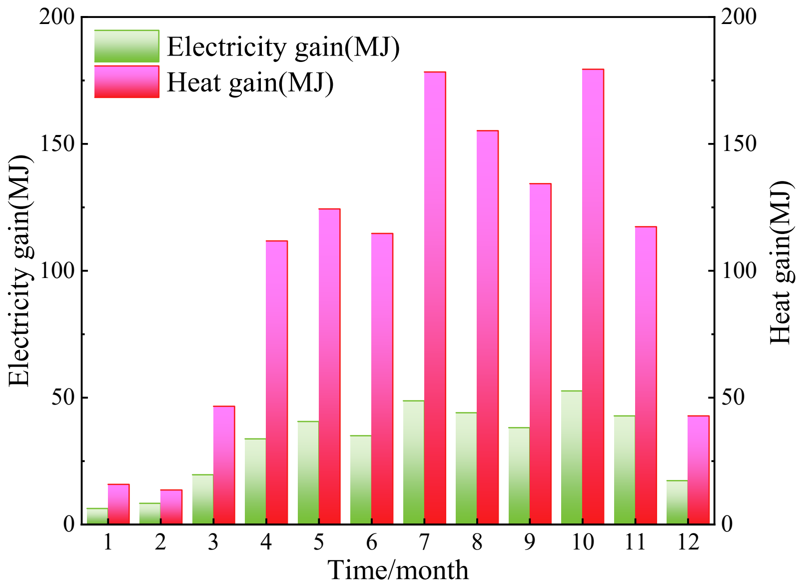

Fig. 19. Electricity gain and heat gain of the HE-PV/T system in Hefei.

Table. 1 All-day system performance comparison between HE-PV/T and FP-PV/T

T_{in} (°C)	Result	Q_{th} (MJ)	Q_{pv} (MJ)	$\eta_{th,a}$ (%)	$\eta_{ele,a}$ (%)	$\eta_{er,a}$ (%)	$\eta_{ex,a}$ (%)
60.0 °C	FP-PV/T	11.88	1.55	26.66	5.24	36.16	6.77
	HE-PV/T	26.86	2.63	39.25	5.74	49.63	8.69
	RISE	14.98	1.08	12.59	0.5	13.47	1.92
70.0 °C	FP-PV/T	8.61	1.63	18.59	5.50	28.56	6.55
	HE-PV/T	21.92	2.59	31.57	5.64	41.78	8.55
	RISE	13.31	0.96	12.98	0.14	13.22	2
80.0 °C	FP-PV/T	5.74	1.47	13.73	5.44	23.60	6.18
	HE-PV/T	16.74	2.55	23.50	5.55	33.55	7.92
	RISE	11.00	1.08	9.77	0.11	9.95	1.74

4.2 Parameter analysis

4.2.1 Influence of the ambient temperature

To evaluate the effect of the ambient temperature on the thermal and electrical performance, other parameters are set as fixed values, such as the rate of mass flow is 0.044 kg/s, the inlet temperature is 60.0 °C, and the solar irradiation is 800 W/m^2. The ambient temperature is raised from 0.0 °C to 35.0 °C. Fig. 20-21 display the system's capacity to generate heat and electricity, as well as its thermal and electrical efficiency. The cooling water is heated by each heat pipe, causing it to gradually warm up along the direction of the flow. When the ambient temperature increases from 5.0 °C to 35.0 °C, the thermal efficiency of the HE-PV/T system improves from 23.27% to 38.83%, while the rise in system temperature leads to a decline in electrical efficiency, which falls from 5.81% to 5.75%. However, this decline in electrical efficiency is far less than the increase in thermal efficiency, so the overall energy utilization efficiency increases from 32.63% to 48.09%. When the FP-PV/T system is under the same working conditions, the overall energy utilization efficiency increases from 24.90% to 43.80% as the ambient temperature rises from 5.0 °C to 35.0 °C, which indicates that the performance of the HE-

PV/T system is greatly improved compared with traditional FP-PV/T system. As shown in Fig. 21, the ambient temperature exerts a positive impact on energy efficiency, but a negative one on overall exergy efficiency. The overall exergy efficiency is decreasing from 8.19% to 7.07% with the increment of ambient temperature from 5.0 °C to 35.0 °C. Although the thermal efficiency is higher at high ambient temperatures, the exergy efficiency may be lower because heat is less useful if the ambient temperature is close to the operating temperature.

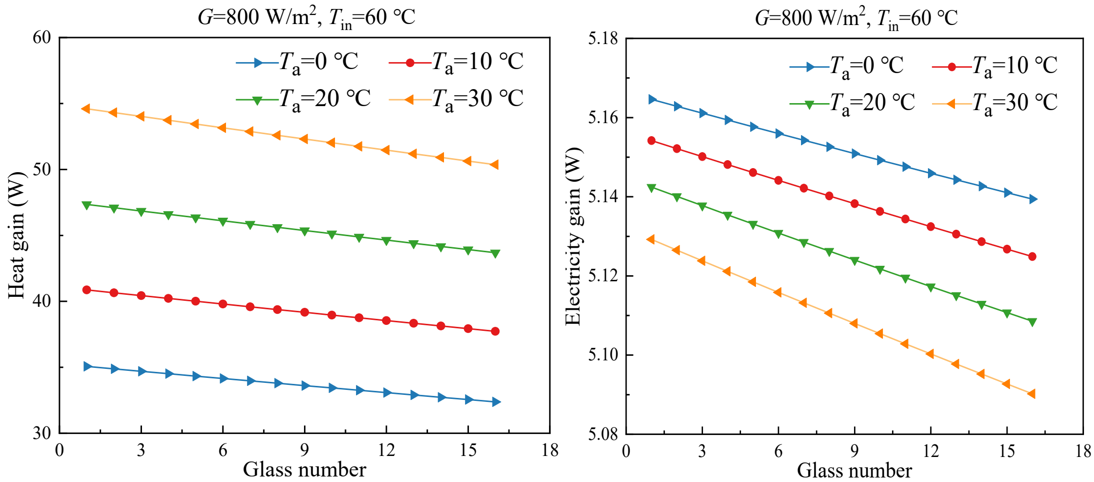

(a) (b)

Fig. 20. Effect of different ambient temperatures on the performance of HE-PV/T system: (a) heat gain of a single tube; (b) electricity gain of a single tube.

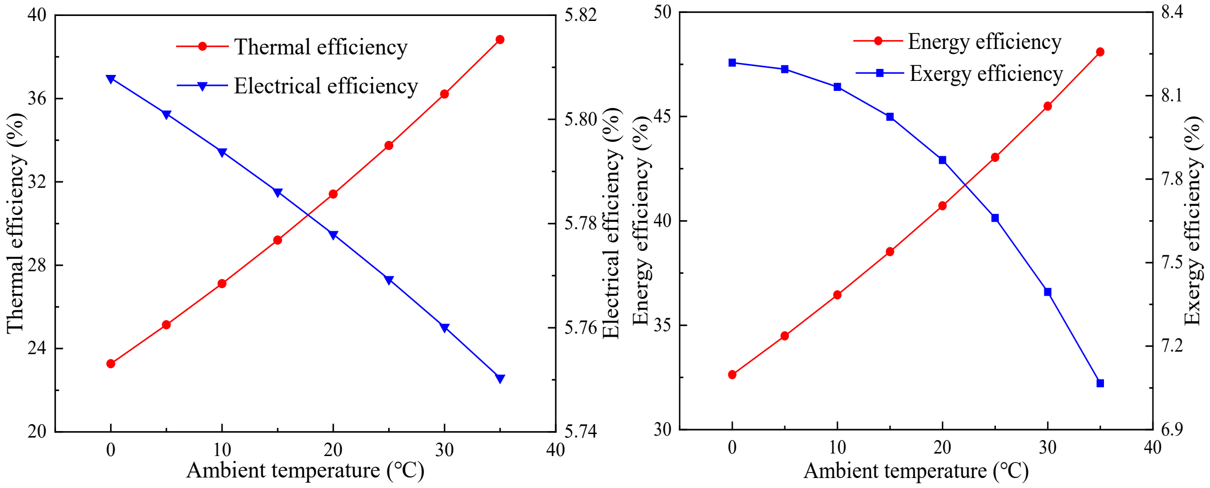

(a) (b)

Fig. 21. Effect of different ambient temperatures on the performance of HE-PV/T system: (a) thermal and electrical efficiency; (b) overall energy and exergy efficiency.

4.2.2 Influence of the solar irradiance

Fig. 22-23 show the thermal and electrical performance of the HE-PV/T system under different solar irradiances. Other factors (the inlet temperature is 60.0 °C, the ambient temperature is 25.0 °C, and the ambient wind speed is 2 m/s) remain constant. An increase in solar irradiance leads to a rise in energy efficiency and exergy efficiency, but the magnitude of the increase decreases gradually. As the solar irradiance increases from 300 W/m^2 to 1000 W/m^2, the thermal efficiency improves from 0.02% to 37.66%, and the electrical efficiency declines almost linearly from 5.90% to 5.72%. And the increment rate of the thermal efficiency decreases gradually along the direction of water flow, and the opposite trend in the decreasing rate of electrical efficiency, which are caused by the power temperature coefficient of a-Si. Moreover, when solar irradiation rises from 300 W/m^2 to 1000 W/m^2, the comprehensive energy efficiency and exergy efficiency increase from 9.53% to 46.87% and from 3.81% to 8.17%, respectively.

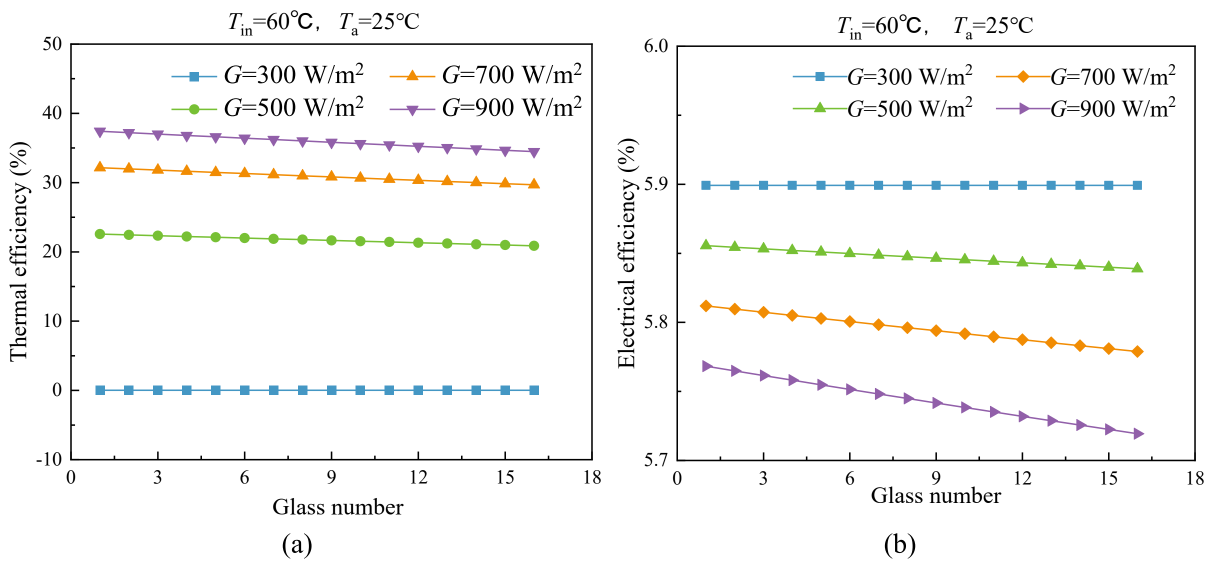

Fig. 22. Effect of different solar irradiances on the performance of HE-PV/T system: (a) thermal efficiency of a single tube; (b) electrical efficiency of a single tube.

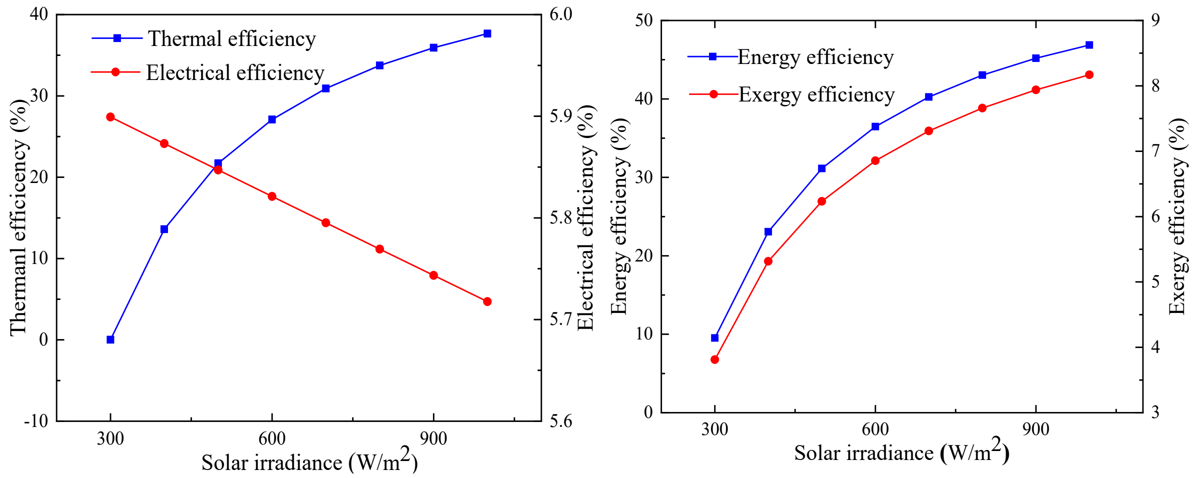

(a) (b)

Fig. 23. Effect of different solar irradiances on the performance of HE-PV/T system: (a) thermal and electrical efficiency; (b) overall energy and exergy efficiency.

4.2.3 Influence of the inlet temperature

The exergy content of thermal energy is related to the operating temperature, so this section studies the effect of inlet temperature on the energy and exergy performance of the HE-PV/T system. The inlet temperature rises from 20.0 °C to 100.0 °C, while the other parameters remain constant (the rate of mass flow is 0.044 kg/s, the ambient temperature is 25.0 °C, the solar irradiance is 800 W/m^2, and the ambient wind speed is 2 m/s). According to simulation research, Fig. 24 illustrates the thermal and electrical efficiency of a single glass tube in the PV/T collector. When the inlet temperature rises by 10.0 °C, both the electrical and thermal efficiency in a single glass tube drop about 0.11% and 5.60%, respectively. As the inlet temperature increases from 20.0 °C to 100.0 °C, Fig. 25 illustrates the thermal and electrical efficiency of the HE-PV/T system drop from 57.88% to 3.85% and from 6.19% to 5.37%, which causes the overall energy efficiency to decrease from 67.85% to 12.51%. When the inlet temperatures are 30.0 °C, 60.0 °C, and 90.0 °C, the comprehensive energy efficiency of the HE-PV/T system is 62.14%, 43.04%, and 20.71%, while the values of the FP-PV/T system are 58.74%, 37.32%, and 14.07%, respectively. Thus, the comprehensive energy efficiency of the HE-PV/T system can be increased by 3.4%, 5.72%, and 6.64% compared with the FP-PV/T collector. The exergy efficiency increases first and then decreases with the increment of inlet temperature, reaching a maximum of 7.66% when the inlet temperature is 60.0 °C. Compared with the FP-PV/T collector which also has a maximum of 7.04% under the same condition, the exergy efficiency of the HE-PV/T system increases by 0.62%.

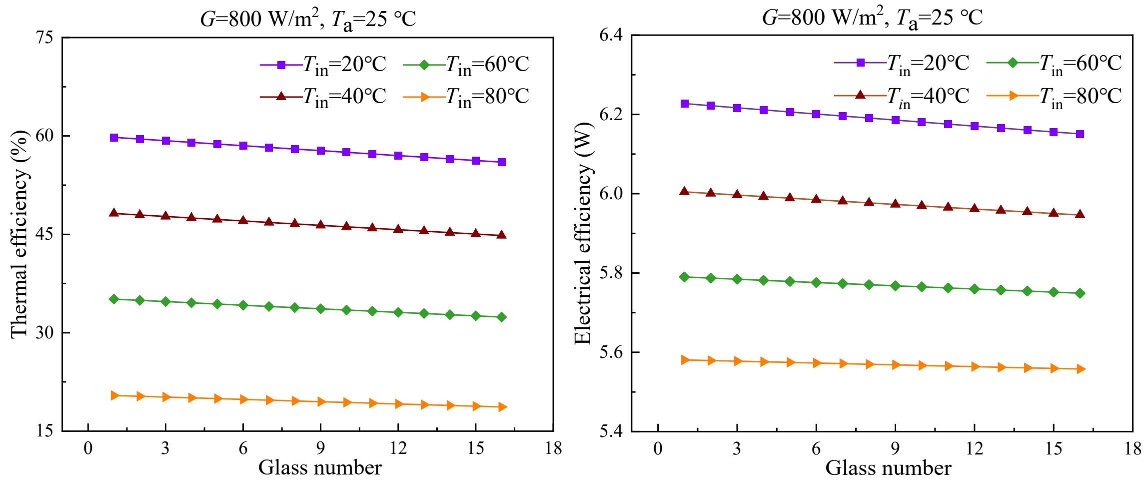

(a) (b)

Fig. 24. Effect of different inlet temperatures on the performance of HE-PV/T system: (a) thermal efficiency of a single tube; (b) electrical efficiency of a single tube.

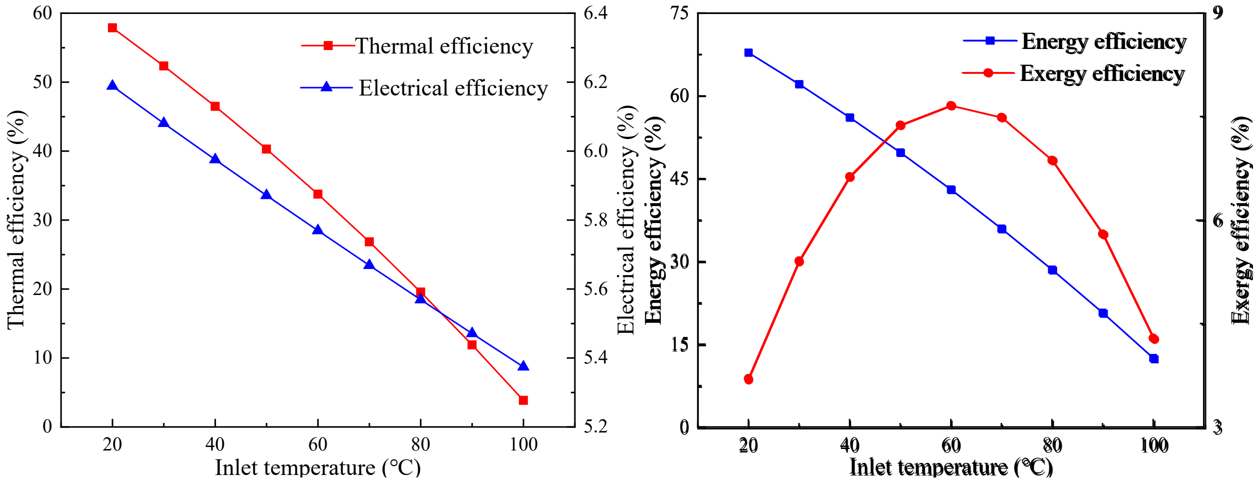

(a) (b)

Fig. 25. Effect of different inlet temperatures on the performance of HE-PV/T system: (a) thermal and electrical efficiency; (b) overall energy and exergy efficiency.

4.2.4 Influence of the mass flow rate

To explore the effect of mass flow on the thermal and electrical performance of the HE-PVT system, the ambient temperature, inlet temperature, solar irradiation, and ambient wind speed are fixed at 25.0 °C, 60.0 °C, 800 W/m^2, and 2 m/s. The influences of the mass flow rate on the thermal efficiency and the exergy efficiency are opposite, while the effect on electrical performance is much weaker than that on the thermal performance, as shown in Fig. 26. When the mass flow rate increases from 0.01 kg/s to 0.05 kg/s, the thermal efficiency and electrical efficiency increase from 25.74% to 32.66% and from 5.67% to 5.78%, respectively. The comprehensive energy efficiency always increases with the increase of mass flow rate, but the exergy efficiency shows a declining phenomenon, because the outlet water temperature drops. When the mass flow rate is 0.01 kg/s and 0.05 kg/s, the overall energy efficiency is 39.95% and 47.14%, and the exergy efficiency is 9.02% and 9.56%. Additionally, Figs. 27-29 indicate that the temperature differences between the PV module and absorber plate are increasing with the mass flow rate rising. When the rate of mass flow increases from 0.01 kg/s to 0.05 kg/s, the maximum temperature of the cell gap decreases from 82.8 °C to 71.5 °C, and the temperature difference of the PV module and the absorber plate increases from 1.0 °C to 1.3 °C and from 0.8 °C to 1.1 °C. These indicate that in the process of mass flow increase, the temperature decreases gradually which is beneficial to the electrical performance, but fortunately, although the temperature distribution of PV cells becomes un-uniform, the change magnitude is small.

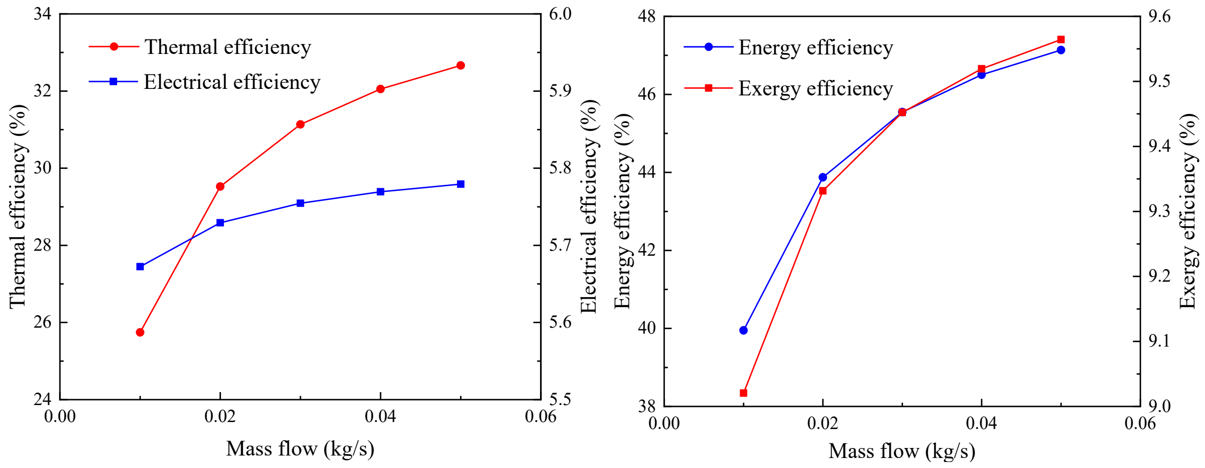

(a) (b)

Fig. 26. Effect of different mass flow rates on the performance of HE-PV/T system: (a) thermal and electrical efficiency; (b) overall energy and exergy efficiency.

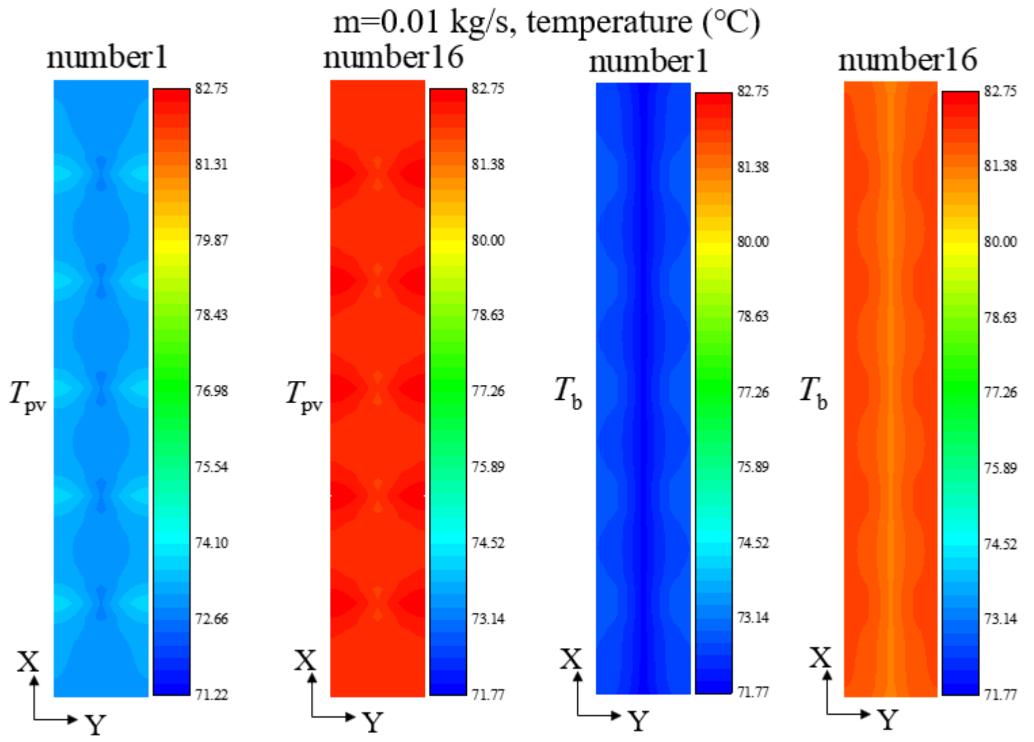

Fig. 27. Temperature distributions of the PV module and the absorber plate: m=0.01 kg/s.

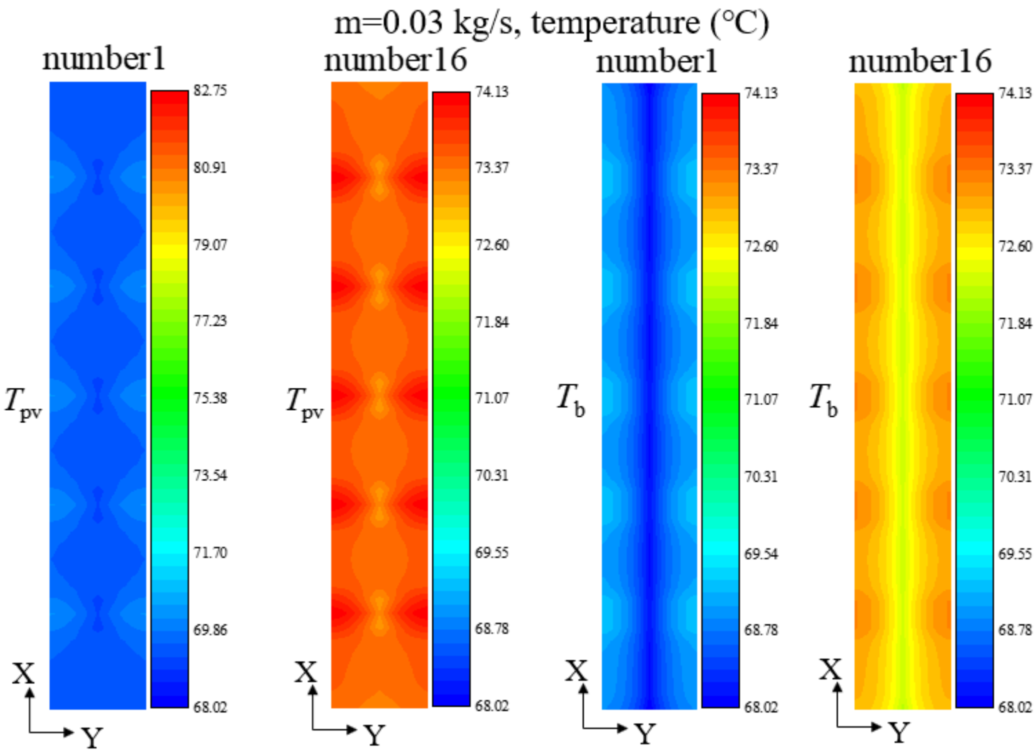

Fig. 28. Temperature distributions of the PV module and the absorber plate: m=0.03 kg/s.

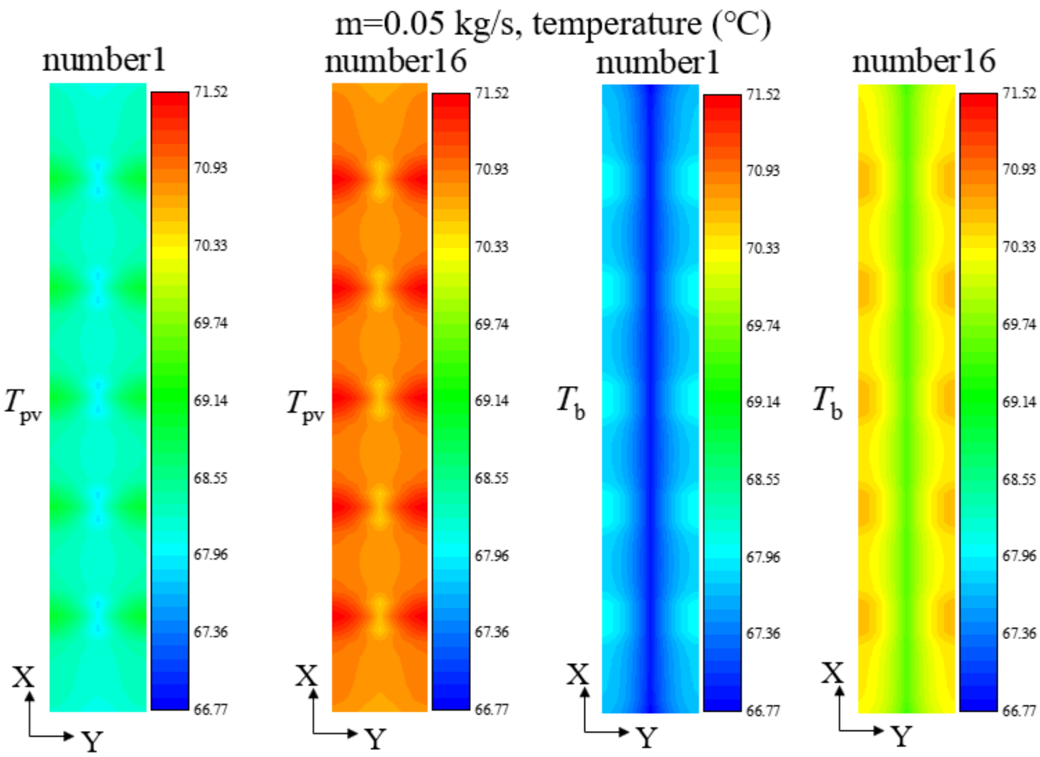

Fig. 29. Temperature distributions of the PV module and the absorber plate: m=0.05 kg/s.

4.2.5 Influence of the coverage rate

The coverage rate of solar cells is an important parameter that influences the thermal and electrical performance of the HE-PV/T system. The solar collection area of the PV/T collector is a fixed value, and the coverage rate is adjusted by changing the area of a-Si cells. Input the inlet temperature of 60.0 °C, ambient temperature of 25.0 °C, and solar irradiance of 800 W/m^2. As the PV cell coverage increases, the total power generation area increases and the electrical gain increases, but the thermal gain decreases due to the conversion of more solar energy into electricity. As shown in Fig. 30, when the PV cell coverage increases from 0.102 to 0.952, the electrical efficiency of the PV cell rises from 5.74% to 5.77%, while the thermal efficiency falls from 41.52% to 33.19%. But, the comprehensive energy efficiency and exergy efficiency have the same trend, when the coverage rate rises from 0.102 to 0.952, the overall energy efficiency is from 43.06% to 47.64%, and the exergy efficiency is from 5.51% to 9.66%. The visual temperature profiles are shown in Fig. 31-33. The smaller the coverage rate, the higher the temperature of each component. When the coverage rate is 0.1, the average temperatures of the a-Si cells layer and aluminum plate are 74.4 °C and 73.7 °C, and the values are 71.9 °C and 71.2 °C at a coverage rate of 0.95, respectively. The temperature differences between the maximum temperature and the minimum temperature of a-Si are 1.2 °C, 0.7 °C, and 0.4 °C when the coverage rates are 0.1, 0.5, and 0.95. Therefore, the temperature distribution is becoming more uniform with the increasing coverage rate.

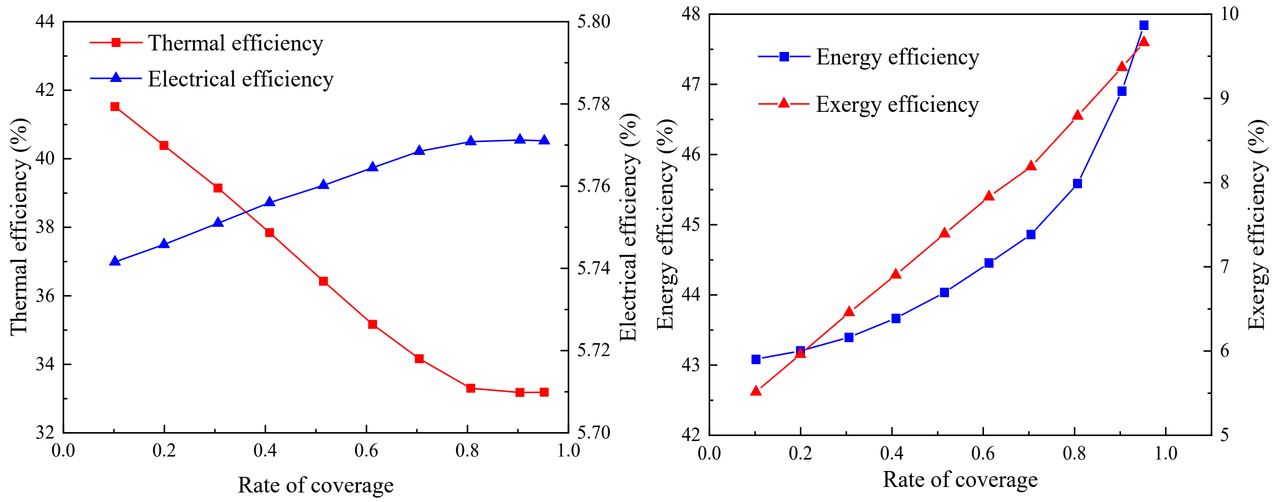

(a) (b)

Fig. 30. Effect of different coverage rates on the performance of HE-PV/T system: (a) thermal and electrical efficiency; (b) overall energy and exergy efficiency.

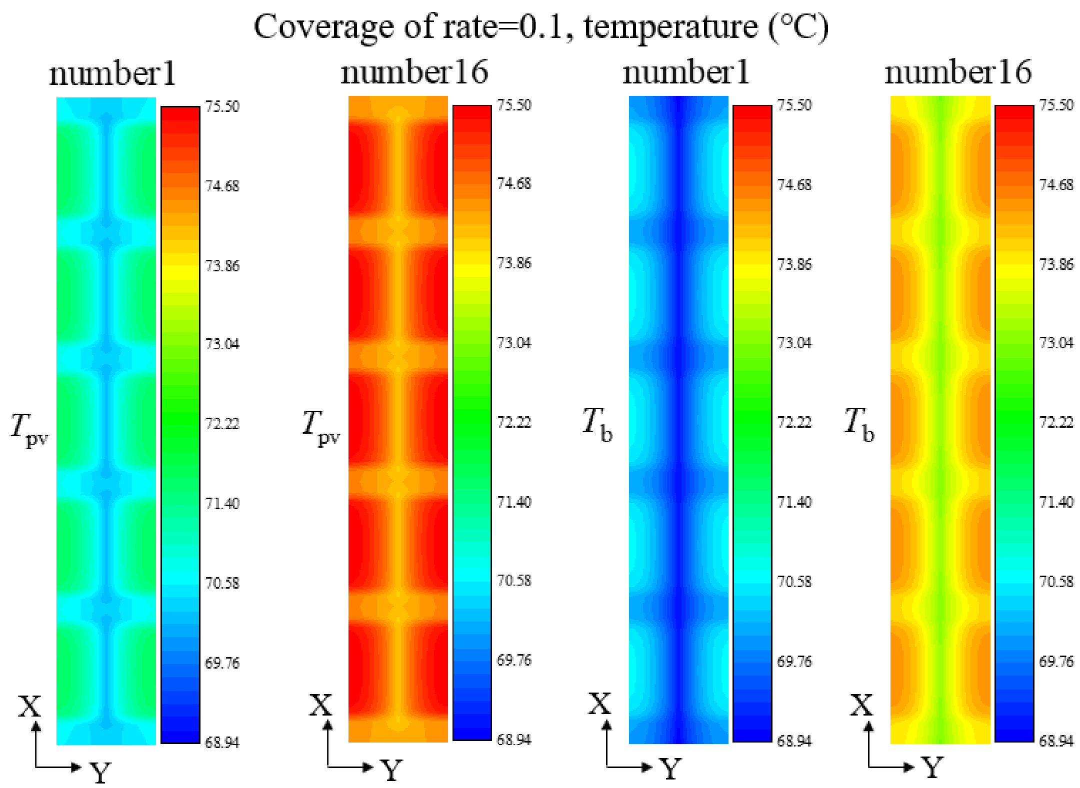

Fig. 31. Temperature distributions of the PV module and the absorber plate: coverage rate of 0.1.

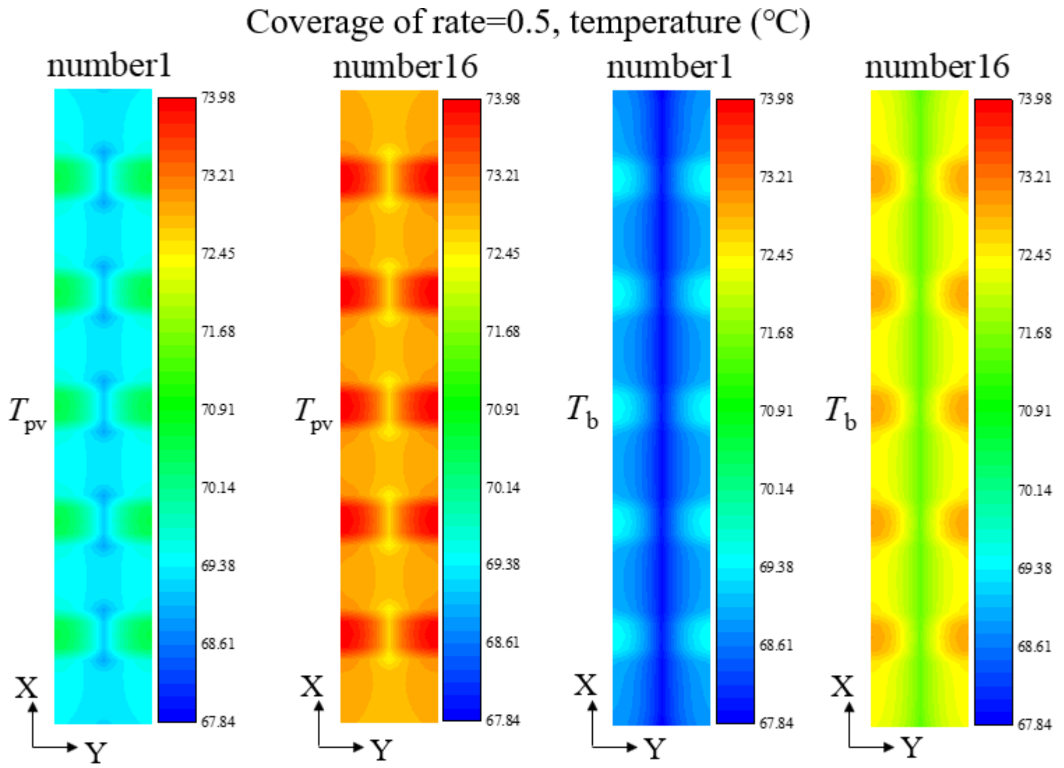

Fig. 32. Temperature distributions of the PV module and the absorber plate: coverage rate of 0.5.

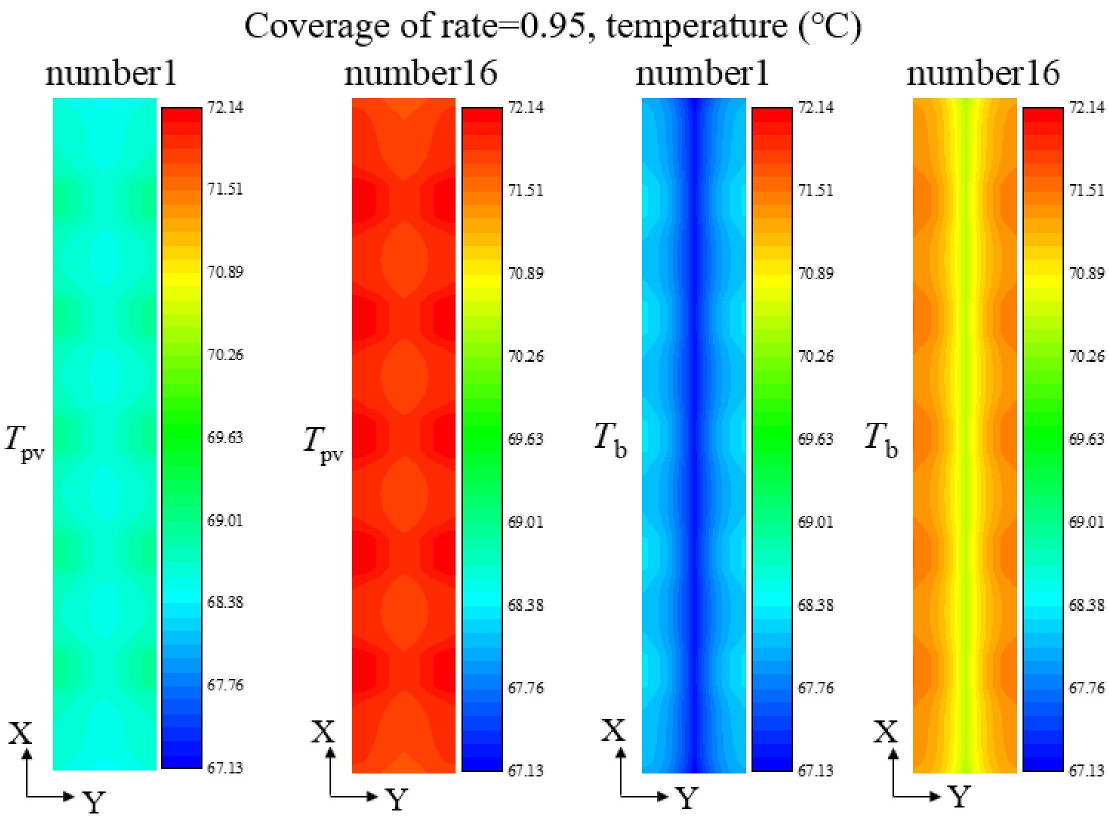

Fig. 33. Temperature distributions of the PV module and the absorber plate: coverage rate of 0.95.

4.3 Economic analysis

To assess the feasibility of the novel HE-PV/T system in terms of finance, an economic analysis of the project is necessary. Net present value (*NPV*) and investment payback period (*PP*) are recognized indicators of economic evaluation for one project, *NPV* is calculated through discounted cash flows minus the initial investment cost, a higher value of *NPV* represents higher availability of the system, and PP is the time taken to gain the total invest of the system, as defined by[47]:

$$NPV = \sum_{i=1}^{n} \frac{CF_i}{(1+r)^i} - IC \tag{48}$$

$$PP = \frac{IC}{averageCF} \tag{49}$$

where, CF_i, *IC,* and LC_{fuel} are the cash flow in individual years of lifetime and initial investment cost, *r i*, and *n* are the discount rate (6.78%)[47], lifetime of investment, and the total lifetime (25 years). Table 2 demonstrates the component cost of the HE-PV/T system[48,49]. It can be seen that PP shown in Fig. 34, the increment of price of energy will cause the payback period of the PV/T system to decline, if only the initial investment cost is required to be recovered without taking into account the additional economic benefits, the EUR 0.087 per kWh will allow the initial investment to return after 25 years of operation of the HE-PV/T system. If the energy price reaches EUR 0.2 per kWh, the initial investment will be repaid in only 11 years and the extra profits will be generated in the remaining 14 years. The *NPV* can clearly indicate the income of the system in the life cycle with the change in energy price. Fig. 34 shows that when the energy price exceeds EUR 0.0406 per kWh, *NPV* of the project is positive and the profit begins to appear. It is believed that subsidies for solar energy from the government increase will lead *PP* to decrease lower and higher *NPV* in the future, under the rapid process of exploiting renewable energy.

Table. 2. Cost of the HE-PV/T system.

Item	price	Item	price
Glass tube (EUR)	212.06	storage battery (EUR)	69.83
Heat pipe (EUR)	210.06	solar tank (EUR)	69.83
a-Si (EUR)	174.58	Pump (EUR)	69.83
Absorber plate (EUR)	184.36		

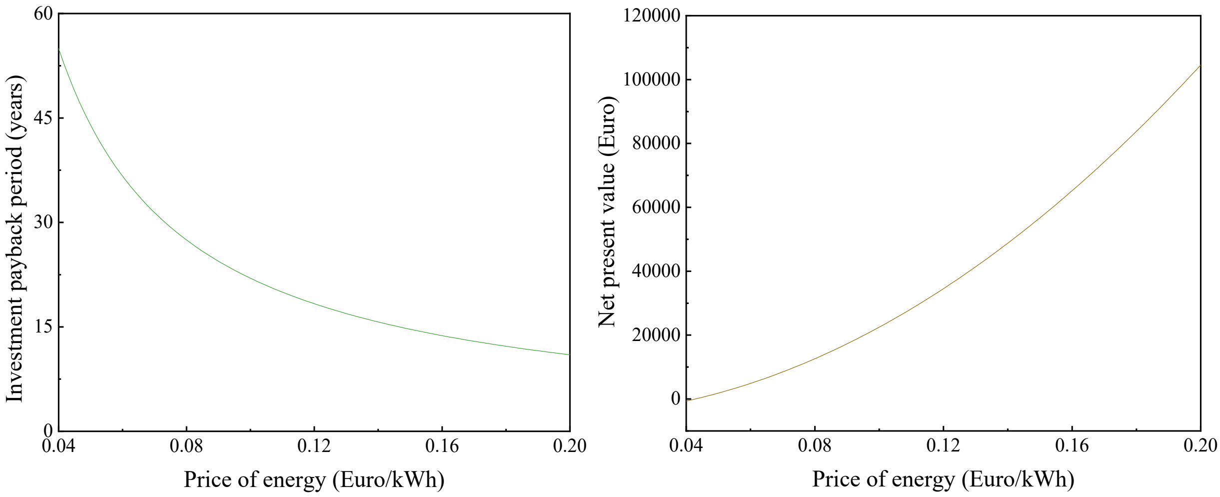

(a) (b)

Fig. 34. System's payback period and NPV under different energy prices.

4.4 Further discussion

While the new HE-PV/T offers a range of advantages in terms of system performance, there will still be inevitable challenges during construction: (1) amorphous silicon cells have not been widely popularized, its photoelectric conversion efficiency is about 8%, up to 10%, while the current market mainstream crystalline silicon cells efficiency is as high as 17% and the price is relatively cheap. (2) Circular tube PV/T, although flexible and convenient for transportation and installation, will cause large area problems.

5. Conclusions

In this paper, a novel heat pipe evacuated tube PV/T system is presented, which aims to increase the efficiency and thermal energy grade of the PV/T system. The heat absorber plate is placed in a full vacuum environment to reduce the convective and conduction heat transfer loss between the absorber plate and the glass cover. A distributed parameter model of the HE-PV/T system is established to investigate the performance and temperature distribution of the system under various conditions. Furthermore, the functioning of the HE-PV/T system's energy flow analysis is carried out. The following succinct summary of the current work's primary findings:

1. The grid independence test of the mathematical model is performed, and 11408 grids are selected considering the accuracy and calculation efficiency. The accuracy of the mathematical model is verified by the experimental results of the heat pipe vacuum tube collector. It is found that the modeling outcomes agree well with the experimental results, and the maximum relative error is 4.35%.
2. When the inlet water temperature is 60.0 °C, 70.0 °C, and 80.0 °C, the maximum comprehensive energy efficiency of the HE-PV/T system reaches 55.20%, 48.68%, and 41.96%. When the inlet temperature is 80.0 °C, the overall energy and exergy efficiency of the HE-PV/T system can reach 33.55%, 7.92%, while the values of the FP-PV/T system are only 23.60%, 6.18%. The improvement of the medium temperature performance of the HE-PV/T system is verified.
3. The environmental parameters that are, ambient temperature, and solar irradiance have a significant impact on the performance of the HE-PV/T system. The ambient temperature exerts a positive impact on energy efficiency, but a negative one on overall exergy efficiency. When solar irradiation

rises from 300 W/m^2 to 1000 W/m^2, the comprehensive energy efficiency and exergy efficiency increase from 9.53% to 46.87% and from 3.81% to 8.17%, respectively.

4. The overall energy efficiency appears a downward trend with the increase of the inlet temperature, but an upward trend with the increase of the mass flow rate. As the inlet temperature increases from 20.0 °C to 100.0 °C, the overall energy efficiency decreases from 67.85% to 12.51%. When the mass flow rate is 0.01 kg/s and 0.05 kg/s, the overall energy efficiency is 39.95% and 47.14%.
5. When the PV cell coverage increases from 0.102 to 0.952, the overall energy efficiency and exergy efficiency increase from 43.06% to 47.64% and from 5.51% to 9.66%, and the electrical efficiency is enhanced from 5.74% to 5.77%, while the thermal efficiency falls from 41.52% to 33.19%. The temperature distribution is becoming more uniform with the increase of the coverage rate, which helps to reduce the mechanical damage caused by the thermal stress of the component operating at medium temperature.
6. After economic analysis, the EUR 0.087 per kWh will allow the initial investment to return after 25 years of operation of the HE-PV/T system, and the price of energy exceeds EUR 0.0406 per kWh, *NPV* of the project is positive and the profit begins to appear.

Acknowledgments

The study was sponsored by National Natural Science Foundation of China (52206292), China Postdoctoral Science Foundation (2022M713463), and the Fundamental Research Funds for the Central Universities (No. 23CX06026A).

Reference

[1] L. El Chaar, L.A. lamont, N. El Zein, Review of photovoltaic technologies, Renewable and Sustainable Energy Reviews 15 (2011) 2165–2175.

[2] P.G. Charalambous, G.G. Maidment, S.A. Kalogirou, K. Yiakoumetti, Photovoltaic thermal (PV/T) collectors: A review, Applied Thermal Engineering 27 (2007) 275–286.

[3] A. Kang, I. Korolija, D. Rovas, Photovoltaic Thermal District Heating: A review of the current status, opportunities and prospects, Applied Thermal Engineering 217 (2022) 119051.

[4] D.T. Cotfas, P.A. Cotfas, S. Mahmoudinezhad, M. Louzazni, Critical factors and parameters for hybrid Photovoltaic-Thermoelectric systems; review, Applied Thermal Engineering 215 (2022) 118977.

[5] M.G. Gado, T.F. Megahed, S. Ookawara, S. Nada, I.I. El-Sharkawy, Potential application of cascade adsorption-vapor compression refrigeration system powered by photovoltaic/thermal collectors, Applied Thermal Engineering 207 (2022) 118075.

[6] A. Abdollahipour, H. Sayyaadi, A review of thermally regenerative electrochemical systems for power generation and refrigeration applications, Applied Thermal Engineering 187 (2021) 116576.

[7] A.H. Shafaghat, M. Eslami, M. Baneshi, Techno-enviro-economic study of a reverse osmosis desalination system equipped with photovoltaic-thermal collectors, Applied Thermal Engineering 218 (2023) 119289.

[8] M. Sheta, H. Hassan, Investigation of multi-effect mechanical vapor compression desalination system powered by photovoltaic/thermal, photovoltaic-evacuated tubes, and photovoltaic solar collectors: Techno-economic study, Applied Thermal Engineering 236 (2024) 121584.

[9] A. Zarei, S. Akhavan, M.B. Rabiee, S. Elahi, Energy, exergy and economic analysis of a novel solar driven CCHP system powered by organic Rankine cycle and photovoltaic thermal collector, Applied Thermal Engineering 194 (2021) 117091.

[10] Q. Li, Q. Hua, C. Wang, A. Khosravi, L. Sun, Thermodynamic and economic analysis of an off–grid photovoltaic hydrogen production system hybrid with organic Rankine cycle, Applied Thermal Engineering 230 (2023) 120843.

[11] S. Aneli, A. Gagliano, G.M. Tina, G. Gediz Ilis, H. Demir, Effectiveness and constraints of using PV/Thermal collectors for heat-driven chillers, Applied Thermal Engineering 210 (2022) 118330.

[12] D. Gao, J. Li, Y. Hao, G. Pei, A novel solar-driven Organic Rankine Cycle system based on the two-stage solar thermal collection and accumulation, Applied Thermal Engineering 234 (2023) 121249.

[13] Performance of a photovoltaic-thermoelectric generator panel in combination with various solar tracking systems, Applied Thermal Engineering 235 (2023) 121336.

[14] C. Lai, C.-H. Su, K. Lin, Analysis of the thermal stress and warpage induced by soldering in monocrystalline silicon cells, Applied Thermal Engineering 55 (2013) 7–16.

[15] P. Yoon, H. Chung, H. Song, J.H. Seo, S. Shin, Investigation of the controlling parameters on the bowing phenomenon in ultra-thin crystalline silicon solar cells, Applied Thermal Engineering 90 (2015) 559–570.

[16] S. Erfantalab, P. Sharma, G. Parish, A. Keating, Thermal analysis of surface micromachined porous silicon membranes using the 3ω method: Implications for thermal sensing, Applied Thermal

Engineering 222 (2023) 119965.

[17]U. Eitner, S. Kajari-Schröder, M. Köntges, H. Altenbach, Thermal Stress and Strain of Solar Cells in Photovoltaic Modules, in: H. Altenbach, V.A. Eremeyev (Eds.), Shell-like Structures, Springer Berlin Heidelberg, Berlin, Heidelberg, 2011: pp. 453–468.

[18]L. Liu, Q. Yu, X. Qi, W. Zhao, G. Zhong, Controlling solidification front shape and thermal stress in growing quasi-single-crystal silicon ingots: Process design for seeded directional solidification, Applied Thermal Engineering 91 (2015) 225–233.

[19]X. Ren, J. Li, M. Hu, G. Pei, D. Jiao, X. Zhao, J. Ji, Feasibility of an innovative amorphous silicon photovoltaic/thermal system for medium temperature applications, Applied Energy 252 (2019) 113427.

[20]X. Ren, J. Li, D. Jiao, D. Gao, G. Pei, Temperature-dependent performance of amorphous silicon photovoltaic/thermal systems in the long term operation, Applied Energy 275 (2020) 115156.

[21]Y. He, Y.B. Tao, H. Chang, Performance analysis and structure optimization for concentrated photovoltaic-phase change material-thermoelectric system in space conditions, Applied Thermal Engineering 232 (2023) 121056.

[22]K. Wang, A.M. Pantaleo, M. Herrando, M. Faccia, I. Pesmazoglou, B.M. Franchetti, C.N. Markides, Spectral-splitting hybrid PV-thermal (PVT) systems for combined heat and power provision to dairy farms, Renewable Energy 159 (2020) 1047–1065.

[23]M. Azizi, R. Tabatabaeekoloor, A. Motevali, S. Reza Mousavi Seyedi, Evaluation of mono and hybrid nano-fluids on energy and exergy parameters of a photovoltaic-thermal system equipped with an eccentric parabolic trough concentrator, Applied Thermal Engineering 223 (2023) 119979.

[24]A. Ustaoglu, V. Akgül, J. Okajima, Performance investigation of truncated low concentrating photovoltaic-thermal systems with V-trough, compound hyperbolic and compound parabolic concentrators, Applied Thermal Engineering 232 (2023) 121028.

[25]D. Gao, G. Gao, J. Cao, S. Zhong, X. Ren, Y.N. Dabwan, M. Hu, D. Jiao, T.H. Kwan, G. Pei, Experimental and numerical analysis of an efficiently optimized evacuated flat plate solar collector under medium temperature, Applied Energy 269 (2020) 115129.

[26]E. Bellos, C. Tzivanidis, A detailed investigation of an evacuated flat plate solar collector, Applied Thermal Engineering 234 (2023) 121334.

[27]A. Radwan, T. Katsura, S. Memon, E.M. Abo-Zahhad, A.A. Serageldin, K. Nagano, Analysis of a vacuum-based photovoltaic thermal collector, Energy Reports 6 (2020) 236–242.

[28]E.M. Abo-Zahhad, S. Ookawara, A. Radwan, A.H. El-Shazly, M.F. El-Kady, M.F.C. Esmail, Performance, limits, and thermal stress analysis of high concentrator multijunction solar cell under passive cooling conditions, Applied Thermal Engineering 164 (2020) 114497.

[29]Y. Zhang, J. Ren, Y. Pu, P. Wang, Solar energy potential assessment: A framework to integrate geographic, technological, and economic indices for a potential analysis, Renewable Energy 149 (2020) 577–586.

[30]Y. Wang, G. Pei, L. Zhang, Effects of frame shadow on the PV character of a photovoltaic/thermal system, Applied Energy 130 (2014) 326–332.

[31]D. Gao, S. Zhong, X. Ren, T.H. Kwan, G. Pei, The energetic, exergetic, and mechanical comparison of two structurally optimized non-concentrating solar collectors for intermediate temperature applications, Renewable Energy 184 (2022) 881–898.

[32]J. Gong, Z. Jiang, X. Luo, B. Du, J. Wang, P.D. Lund, Straight-through all-glass evacuated tube

solar collector for low and medium temperature applications, Solar Energy 201 (2020) 935–943.

[33] Q. Sun, Z. Xue, Y. Chen, R. Xia, J. Wang, S. Xu, J. Zhang, Y. Yue, Modulation of the thermal transport of micro-structured materials from 3D printing, Int. J. Extrem. Manuf. 4 (2022) 015001.

[34] L. Das, N. Aslfattahi, K. Habib, R. Saidur, K. Irshad, S.M. Yahya, K. Kadirgama, Improved thermophysical characteristics of a new class of ionic liquid + diethylene glycol/Al2O3 + CuO based ionanofluid as a coolant media for hybrid PV/T system, Thermal Science and Engineering Progress 36 (2022) 101518.

[35] S.W. Churchill, M. Bernstein, A Correlating Equation for Forced Convection From Gases and Liquids to a Circular Cylinder in Crossflow, Journal of Heat Transfer 99 (1977) 300–306.

[36] J.A. Duffie, W.A. Beckman, Solar Engineering of Thermal Processes, (n.d.).

[37] H.M.S. Hussein, M.A. Mohamad, A.S. El-Asfouri, Optimization of a wickless heat pipe at plate solar collector, Energy Conversion (1999).

[38] Fundamentals of Heat Exchanger Design, (n.d.).

[39] D.I. Jung, C. Chow, A. Wu, The role of transformational leadership in enhancing organizational innovation: Hypotheses and some preliminary findings, The Leadership Quarterly 14 (2003) 525–544.

[40] L. Zalewski, Experimental thermal study of a solar wall of composite type, (n.d.).

[41] P. Gang, F. Huide, Z. Huijuan, J. Jie, Performance study and parametric analysis of a novel heat pipe PV/T system, Energy 37 (2012) 384–395.

[42] D.T. Cotfas, P.A. Cotfas, O.M. Machidon, Study of Temperature Coefficients for Parameters of Photovoltaic Cells, International Journal of Photoenergy 2018 (2018) 1–12.

[43] J. Ji, J.-P. Lu, T.-T. Chow, W. He, G. Pei, A sensitivity study of a hybrid photovoltaic/thermal water-heating system with natural circulation, Applied Energy 84 (2007) 222–237.

[44] M. Gholampour, M. Ameri, Energy and exergy analyses of Photovoltaic/Thermal flat transpired collectors: Experimental and theoretical study, Applied Energy 164 (2016) 837–856.

[45] C.-J. Kat, P.S. Els, Validation metric based on relative error, Mathematical and Computer Modelling of Dynamical Systems 18 (2012) 487–520.

[46] X. Huang, Q. Wang, H. Yang, S. Zhong, D. Jiao, K. Zhang, M. Li, G. Pei, Theoretical and experimental studies of impacts of heat shields on heat pipe evacuated tube solar collector, Renewable Energy 138 (2019) 999–1009.

[47] M. Libra, D. Mrázek, I. Tyukhov, L. Severová, V. Poulek, J. Mach, T. Šubrt, V. Beránek, R. Svoboda, J. Sedláček, Reduced real lifetime of PV panels – Economic consequences, Solar Energy 259 (2023) 229–234.

[48] A. Gagliano, G.M. Tina, S. Aneli, S. Nižetić, Comparative assessments of the performances of PV/T and conventional solar plants, Journal of Cleaner Production 219 (2019) 304–315.

[49] L. Wu, B. Zhao, X. Ao, H. Yang, X. Ren, Q. Yu, K. Guo, M. Hu, G. Pei, Performance analysis of the aerogel-based PV/T collector: A numerical study, Solar Energy 228 (2021) 339–348.